Gutiérrez-Moizant, R., Ramírez-Berasategui, M., Sánchez-Sanz, S., & Santos-Cuadros, S. (2020). Experimental verification of the boundary conditions in the success of the Brazilian test with loading arcs. An uncertainty approach using concrete disks. *International Journal of Rock Mechanics and Mining Sciences*, 132, 104380.

DOI: 10.1016/j.ijrmms.2020.104380

Experimental verification of the boundary conditions in the success of the Brazilian test with loading arcs. An Uncertainty approach using concrete disks.

R. Gutiérrez-Moizant[1]*, M. Ramírez-Berasategui[1], S. Sánchez-Sanz and S. Santos-Cuadros[1]
[1]Mechanical Engineering Department, Universidad Carlos III de Madrid, Leganés, Madrid 28911, Spain.
*Corresponding author: Universidad Carlos III de Madrid, Avenida de la Universidad n°30, Leganés, Madrid 28911, Spain.
Email: ragutier@ing.uc3m.es

Abstract

The present work analyses the reliability of the Brazilian test with loading arcs. A new testing set up has allowed to determine in an effective way the real load of the failure initiation as this moment was not always or correctly detected by the universal testing machine. The instrumentation used is a simple and low-cost method that allows to know the possible pressure distribution in the contact zone as well as the final contact angle. It has been observed that the success of the test depends mainly on the surface finish of the parts involved, their geometric tolerances and the symmetry of the applied load. These boundary conditions have a direct effect in the contact pressure distribution. The possible failure modes observed experimentally have been simulated with the finite element methods. For this, the contact boundary condition has been changed and the possible stress distribution in term of Griffith equivalent stress has been obtained. The numerical analysis allows to study the influence of the initial contact condition on the success of the test and agrees with the experimental results. Furthermore, an uncertainty analysis in the expression of the tensile strength confirms that, when the test is valid, a crack appears suddenly in the central area of the disk, as observed experimentally, so there is no need to determine if the starting point is in the centre. Additionally, it has been observed that the initial crack length depends on the type of pressure distribution in the contact zone. Finally, a series of recommendations are given in order to minimize both the variability of the final contact angle and the risk of premature failure of the Brazilian disk.

Keywords: Brazilian disk, indirect tensile strength, contact pressure distribution, crack initiation, load failure.

1. Introduction

The tensile strength of rock and concrete is necessary to predict their mechanical behaviour.[1] There are methods to measure directly the uniaxial tensile strength (direct methods) and others in which this parameter is measured indirectly (indirect methods). A direct tensile test is conducted by applying an axial tensile force to the specimen. However, the direct determination of the tensile strength is difficult to perform.[2] This has promoted the development of simpler tests using indirect methods, as the uniaxial compressive strength test, the diametrical compression of disks and rings, and the three- or four-point bending test.[3] However, these indirect methods are usually criticised since their proposal,[4] because the stress field produced is far from being uniaxial in the majority of cases.[5]

The uniaxial tensile test has a few weaknesses:[6,7] the possible eccentricity of the load and the additional stress of the holding devices combined with the quasi-brittle nature of the material. Meanwhile, the Brazilian test is the most popular indirect tensile strength method for brittle materials.[8] In this test, a circular disk is diametrically compressed until its failure, in such a way that its compression induces tensile stresses normal to the vertical diameter. It was initially proposed by Carneiro[9] and, later, analytically solved by Hondros[10] for isotropic rocks.

The Brazilian test was officially proposed in 1978 by the International Society for Rock Mechanics (ISRM) as a method to determine the tensile strength of rock materials.[11] This standard uses two steel loading jaws with an internal radius of R_j=1.5R, where R is the radius of the disk-shaped specimen. The rock failure follows the Griffith criterion[12] or the maximum tensile stress criterion (when the initial crack point is in the centre of the disk, these two criteria are equivalent). This is valid as long as the compressive strength is much greater than the tensile strength. If the ratio between compressive and tensile strengths decreases, the determination of the indirect tensile strength is less performant due to a higher probability of failure in the contact zone.[4]

The theoretical considerations of Brazilian test involve the following assumption:[5]

- The material of the disk is homogeneous, isotropic and linear elastic.
- The contact length between the specimen and the loading jaws is a finite arc rather a single point.
- The contact is simulated by a uniform radial compressive pressure acting on two arcs, symmetric with respect to the centre of the disk.
- The only stress in the contact is a radial compression.

- Any friction forces between the disk-jaws interface are ignored.
- The problem is modelled assuming a plane-stress behaviour.

Nevertheless, these assumptions are difficult to reproduce experimentally.[7,13] According to the Griffith criterion, the crack initiation has to be in the centre of the disk to ensure that the maximum transverse stress corresponds to the uniaxial tensile strength.[7] The range of contact angles recommended by the ISRM[11] does not seem to meet the Griffith's criterion, as it has been demonstrated that the failure, for these angles, can be located near the loading zone.[7,14–16] This would invalidate the test for the determination of the tensile strength.

To reduce the stress concentration on the loading area, Jaeger and Hoskins[17] proposed to use loading arcs (**Figure 1b**) instead of the classical ISRM jaws (**Figure 1a**), in order to improve the control of the contact angle. However, Mellor and Hawkes[18] disapproved this jaw configuration, because the arc ends can penetrate the disk and invalidate the test. Years later, Yu et al.[19] experimentally proved that when the contact angle is larger than 20º, the crack starts in the centre of the disk and the dispersion of the final tensile strength is small. Additionally, Erarslan et al.[6] observed that when the loading arcs are used, the central failure of the disk is guaranteed for $20º \leq 2\alpha \leq 30º$.

Alibadian at al.[20,21] demonstrated that when wooden cushions are placed between a flat loading plate and the disk, the load transfer and the failure procedure occur more gradually than in the classical Brazilian test with flat platens. Moreover, they concluded that the premature disk failure is avoided if the contact angle $2\alpha \geq 15º$. However, the load distribution generated with this new experimental set up has not been analysed yet. Additionally, the authors observed through Digital Image Correlation techniques (DIC) that the crack might initiate in the disk centre, or somewhere between the contact zone and the centre. It is important to note that the authors did not observe a crack initiation point but a first line crack location.

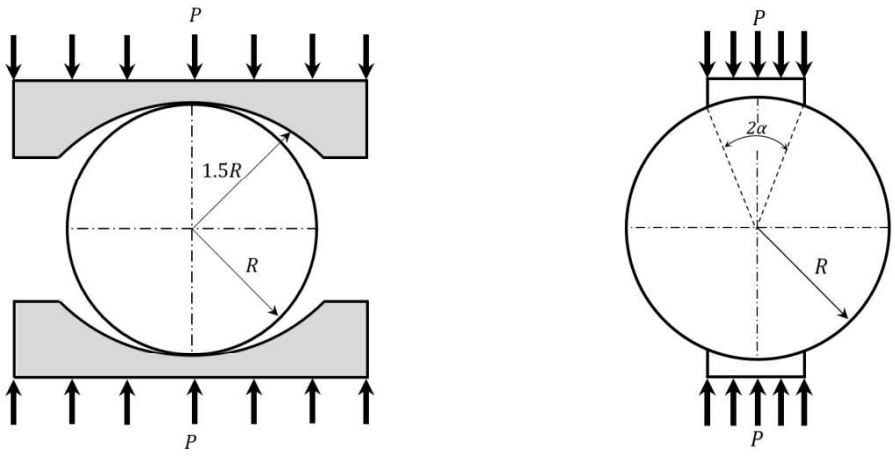

Figure 1 a Brazilian test with a classical jaws and **b** with loading arcs

There are different boundary conditions that can affect to the crack initiation.[7] The contact angle between the jaws (loading device) and the disk specimen plays a significant role, since this is strongly related to the location of the crack initiation point.[6,22] The role of friction stresses has also been treated in several researches[23,24] and they concluded that the influence of the contact friction on the stress at the centre of the disk can be neglected if a uniform radial load is applied. Otherwise, its influence cannot be neglected under the loading edge. Moreover, the success of the indirect tensile test depends on the specimen material and its composition.[25,26] The presence of an initial defect in the specimen can lead to a premature failure.[27]

Therefore, despite being a testing method widely used to determine the tensile strength of rocks and concrete, there are nowadays some unsolved questions related to the Brazilian test:[6]

- What is the value of the real contact angle at the time of the disk failure?
- How to observe experimentally the crack initiation point.
- Is there a low-cost and easy to use technique to detect with precision the load at the crack initiation?

For the study of crack initiation and propagation, several researches[6,7,28–34] concluded that numerical simulation methods (Finite Element Methods or Discrete Elements Method) are a good tool to analyse the crack initiation process.

On the other hand, non-contact measurement techniques, such as Digital Image Correlation (DIC) in combination with high-speed photography are a promising tool to verify the validity of the Brazilian test.[35–40] Moreover, high-speed cameras are the most convenient way to capture the failure process.[41] However, some authors[36] concluded that even with high acquisition frequency systems, it is difficult to observe and

identify the crack initiation. The acoustic emission technique (AE) [42,43] has also been used to study the failure process in the Brazilian test and is useful to detect the premature failure of the disk and the failure load. To guarantee a successful signal detection with the AE, a layer of grease is applied to the area sensor in contact with the disk to improve the coupling effect. Usually, the sensors are secured by rubber bands or steel clamp to the disk[43,44]. However, the signal detection during the test can be seriously influenced by the texture of the rock[43] and the noise due to the deformation on the zone where the sensors are in contact with the disk, causing thus their relative movement.

Additionally, several research works[8,14,42] advise that the magnitude of the load at the first crack detection can be different to the final failure load. Therefore, a false indirect tensile strength could be obtained.

This research work aims to determine the characteristics under which the test with loading arcs is successful. To do so, the questions mentioned above will be considered by performing an experimental test with 12 concrete disks of different composition using an instrumented loading arc. Moreover, the quantification of the uncertainties for the possible theoretical solutions, allows to explain why it is so complex to experimentally observe the crack initiation point in the Brazilian disk.

2. Experimental study

2.1. Material

A series of indirect tensile tests with a 30º loading arc were carried out with high strength concrete disks of diameter 150 mm. It was chosen to use concrete instead of rock in order to have a disk with an adequate size that allows to analyse the possible distribution of pressure on the contact. Three groups of four concrete disks with different designs of mixtures were elaborated. The first group corresponds to a mix design with a compressive strength above 80 N/mm^2 (grade M80). In the first samples of the concrete group, the water/cement ratio varies from 0.2 to 0.3, the fine aggregate used is river sand with a density of 2.60 g/cm^3 and the coarse aggregate is crushed limestone with a maximum size of 6 mm. A 52.5 N CEM I portland cement was used according to the European standard EN 197-1:2011.[45] A silica fume concentration of 9% of the total cementitious material was introduced into the mix design to improve the sample performance. In addition, a superplasticizer of 1% of the weight of the cement was used. The concrete disks for the second and third groups were made with the same mixing formula as the first group, but with 20% and 33% more river sand, respectively. Due to the composition (cement with fragments of rock and sand), the concrete disks analysed could be considered as a type of artificial rock similar to sedimentary rocks as sandstone or shale.[46,47] The variation of the sand content is a way to analyse how it affects to the mechanical behaviour of concrete and to the success of the test. Moreover, it introduced uncertainties in the concrete mix, as they are not marked by the standards. This variability of composition also happens in nature with sedimentary rocks.

The dimensional characteristics of the concrete disks are shown in **Table 1**. Each dimension is provided with its combined uncertainty. The latest was calculated according to the Guide to the expression of uncertainty in measurement (GUM).[48] Therefore, it takes into account the standard uncertainty of the mean and the uncertainty of the calliper used for the measurements ($u(t) = u(D) = 2.89\times10^{-2}$ mm) for a confidence level of 95%.

Table 1. Dimensional characteristics of the concrete disks

Group number	Disk number	Diameter (mm)	Thickness (mm)
Group I	D_I1	149.97 ± 0.19	75.71 ± 0.46
	D_I2	150.26 ± 1.19	75.90 ± 0.45
	D_I3	150.05 ± 0.48	75.97 ± 0.25
	D_I4	149.92 ± 1.10	75.89 ± 0.33
Group II	D_II1	149.26 ± 1.42	75.76 ± 0.25
	D_II2	149.77 ± 1.23	75.72 ± 0.64
	D_II3	149.83 ± 0.84	75.40 ± 0.34
	D_II4	149.99 ± 1.16	75.57 ± 0.55
Group III	D_III1	150.65 ± 0.78	75.72 ± 0.20
	D_III2	150.12 ± 1.18	75.60 ± 0.68
	D_III3	150.65 ± 1.38	75.76 ± 0.33
	D_III4	150.20 ± 1.17	75.00 ± 2.22

2.2. Splitting test

The indirect tensile tests were carried out using an electro-mechanic testing machine class II.[49] The test was conducted in the controlled loading mode with a rate of 200 N/s according the suggestion given by the ISRM.[11] The disks were compressed by two loading arcs of 30º in order to avoid premature failure, following the recommendations published in previous articles.[6,8,14] The disks tested do not have exactly the same dimensions as it can be seen in **Table 1**, so it has been necessary to design the jaws or loading arcs considering the geometric tolerance of the studied sample. Thus, the final dimensions of the loading arcs are 75.57 mm for the radius and 76.6 mm for the thickness. These dimensions correspond to the maximum values measured in the sample, so that it can be ensured that all the disks fit into the loading arcs.
The loading arcs are manufactured from an S355 steel cylinder. The type of steel selected guarantees the structural rigidity of the loading device and complies with the requirements of the ISRM.[11]

In order to verify the final contact angle, the top loading arc has been instrumented with five 2 mm-grid length stacked rectangular rosettes bonded on the edge of the arc and aligned with the transverse and radial directions. Moreover, the strain gauges will also allow to determine the possible pressure distribution near the contact zone. For the gauges a 3-wire configuration and ¼ bridge has been used. The recording of the force, displacement and strain has been made with the equipment that controls the testing machine. The sampling frequency of all the variables involved was 10 Hz. **Figure 2** shows the instrumented loading device and the experimental set-up.

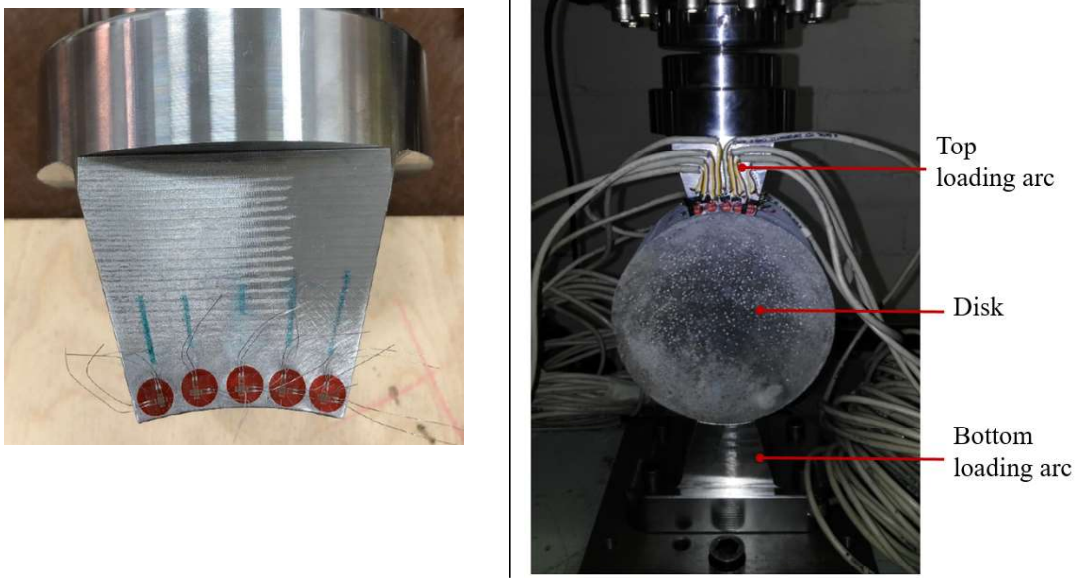

(a) **(b)**

Figure 2 Testing design: **a** instrumented top loading arc and **b** Experimental set up

The crack initiation point in the disks, was recorded with a Photron high-speed camera, model SA3. The recording speed has been set at 2000 fps with a resolution of 1024 x 1024 pixels. Due to the characteristics of the camera and the quality of the image, the recording time is very limited. Once the crack has been detected, the recording mode is activated manually. The camera can record everything that has happened eight seconds before the image capture is triggered. Thus, it has been possible to detect the exact moment of the beginning of the disk failure.

In every manufacturing process, there are inaccuracies that affect to the quality of the final product. In the case studied, this implies that the contact between the disks and the loading device may not complete at the beginning of the test. Because of this, it was made sure in all the tests that the initial contact between the disks and the loading arcs was as high as possible. To do this, the disk was rotated until the zone of best contact with the loading device was detected. However, for the disk D_II3, an incomplete initial contact was set up in order to verify how this affects to the validity of the test. **Figure 3** shows an example of a complete and uncompleted initial contact between two of the disks and the top loading arc.

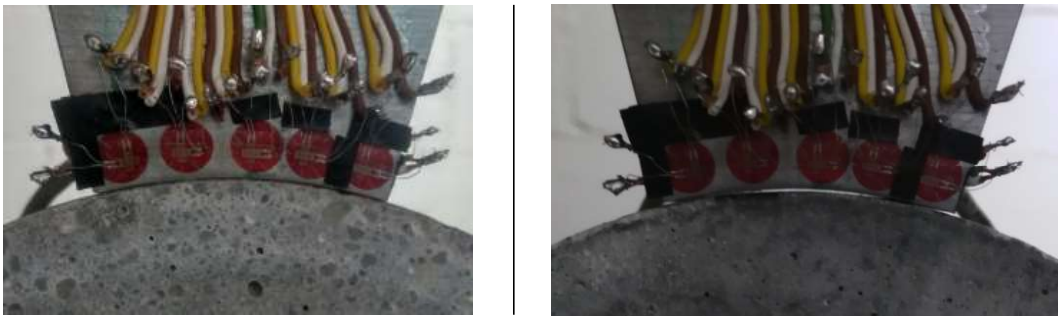

(a) **(b)**

Figure 3 Initial boundary condition in the contact area: **a** Disk D_I4 **b** Disk D_III1

2.3. Brazilian test for verification of optimal test conditions

The verification of the optimal test conditions was also carried out using an F114 steel disk. The disk was manufactured with a radius equal to the one of the loading arcs, in order to recreate the condition of complete contact from the beginning of the test. Additionally, the disk was instrumented with three stacked rectangular rosettes of 6 mm-grid length, aligned with the transverse and radial direction and bonded along the loading radius. This strain gage rosette will allow to analyse the effect that the contact conditions have on the result of the stress in the disk. **Figure 4** shows the experimental set-up and the initial contact condition in the Brazilian test with the steel disk and loading arcs.

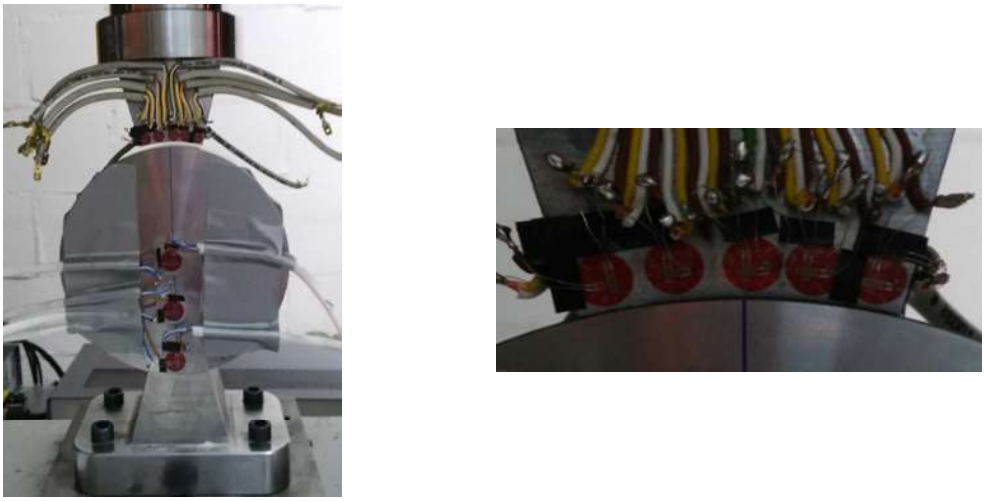

(a) **(b)**

Figure 4 a Experimental mounting and **b** initial boundary condition in the contact area of the Brazilian steel disk

The compressive strengths of the Brazilian steel disk were tested with the load rate recommended by the ISRM standard.[11] The transverse and radial stresses were calculated using the biaxial form of Hooke's law [50]. A Young modulus of 211 MPa ± 1% and Poisson ratio of 0.3 ± 0.5% were considered for the F114 steel. The elastic properties were calculated from flat specimens of the same material that the disk following the recommendations given by ASTM.[51,52]

3. Numerical modelling

Several research studies performed so far prove that the Finite Element Method (FEM) can effectively recreate the indirect test in its different configurations.[6,7,14,53] In order to check the final contact angle and the possible crack initiation point, the indirect tensile test was modelled with the commercial software Abaqus as a two-dimensional plane strain models considering the literature review.[6,53] The material properties were supposed of elastic and homogeneous behaviour. The loading arcs have been included in the model with the material properties of the steel (Young's modulus of 210 GPa and Poisson's coefficient of 0.33). The loading arcs materials selected guarantee the stiffness of the loading device and is in agreement with the requirement given by the ISRM.[11] The contact between the loading arcs and the disk was simulated using the surface-to-surface contact algorithm with a friction coefficients of 0.5, according the state of the art.[54] The approach considers the shape of the contact geometries and provides more accurate results than a node-to-surface discretization in surface geometry without irregularities, such as crests and

troughs.[55] The contact conditions were defined over a finite region instead of at each node, which tends to minimize contact problems, as the master surface (in our case loading arc) penetrates the slave surface (Brazilian disk). This is appropriate in simulation models where the normal direction of the surfaces in contact are opposite, as is the case of the Brazilian test.

The finite-sliding contact formulation was selected in order to continually update which part of the master surface (loading arc) is in contact with each slave node (disk) as the compression force is applied. A minimum tolerance of 0 mm for the surfaces in contact was specified, avoiding the probable converge problems due to overclosed nodes.[55] The loading device was meshed with 4-node bilinear plane strain quadrilateral elements of size 0.5 mm. The disk was modelled with the same element type and size than the loading arc, except in the contact zone where the size of the elements was 0.1 mm, in order to analyse the effective contact angle. The mesh size used guarantees the convergence of the solution with respect to the mesh refinement. A uniform pressure was applied to the flat surface of the top loading arc, while the bottom one was completely fixed in the lower face (**Figure 5**). The disk has a diameter of 151.14 mm and a thickness of 76.6 mm.

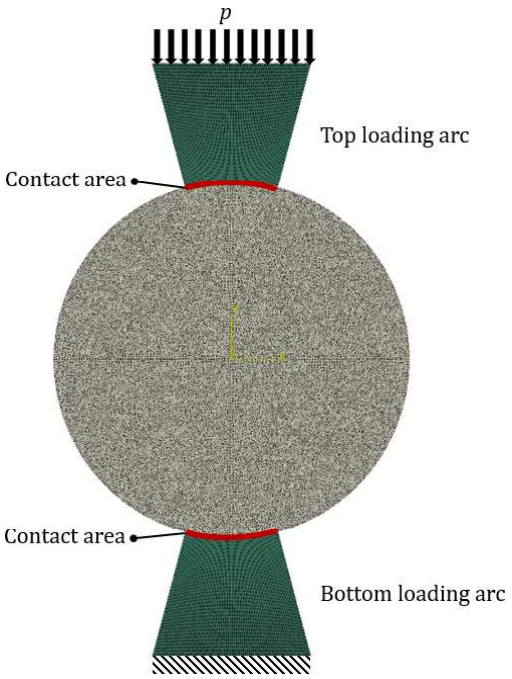

Figure 5 Numerical indirect test with loading arcs of 30º

The simulations were carried out considering the possible variations of the mechanical properties of the material and the inaccuracy between the radii ratio of the loading arcs and the concrete disks (ρ = radius of the arcs/radius of the disk). For this purpose, a central composite design[56] has been made, considering ranges of variation for the Young's modulus (30-70 MPa), the Poisson's coefficient (0.2-0.3), the tensile strength (4-8 MPa) and the ratio between radii (1.008-1.02). Smaller radii ratios are not possible as the disk would not fit into the arc of the loading device, but bigger ratios would imply an initial smaller contact angle than the loading arc. In order to guarantee the stability of the numerical models, it has been decided to modify the radius of the loading arcs instead of the one of the disks, according to the ρ values analyzed. In this way, it is not necessary to re-mesh the disk as ρ values change, avoiding the influence this can have on the precision of the numerical results. **Table 2** shows the levels used for the input parameters. The simulation stops when the maximum tensile strength value has been reached.

Table 2. Data set for the Central Composite Design for the numerical Brazilian test

E (GPa)	ν ($\mu\varepsilon/\mu\varepsilon$)	σ_t (MPa)	ρ (mm/mm)
10	0.15	2	1.002
30	0.2	4	1.008
50	0.25	6	1.014
70	0.3	8	1.020
90	0.35	10	1.026

4. Experimental results

4.1. Validity of the tests and load failure

In the present research work, it has been observed that the use of this type of compression jaws does not guarantee that the effective contact angle is equal to the loading arc. During the test, it is possible to know the effective contact angle if the test is stopped just when the first crack appears, although this is not always possible since the speed of propagation of the crack is uncertain. Moreover, a clear transition has been observed between the surface texture of the disk in the contact zone and the rest of the surface. The marks between the texture changes allow to measure the arc length, and thus, the effective contact angle. **Figure 6** shows the marks observed in the contact zone of one of the disks tested.

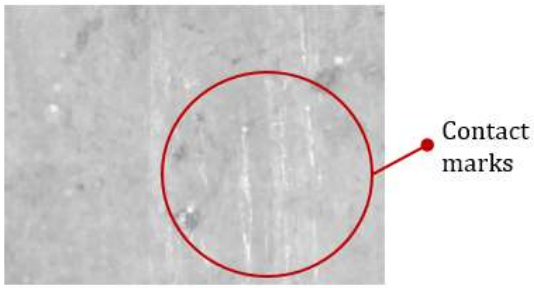

Figure 6 Marks observed in the contact zone of the disk

Table 3 shows the arc length measured on the disk surface at the end of the test and the effective contact angles calculated with that length, except for disk D_II1 where the contact angle could not be measured because the failure speed was of such magnitude that it destroyed the sample completely.

Table 3. Effective contact angle calculated from the measurement of the length of the contact arc

Group number	Disk number	ρ (mm/mm)	Arc length (mm)	Efecctive contact angle (º)
Group I	D_I1	1.007	39.3	30.0
	D_I2	1.006	34.0	25.9
	D_I3	1.007	38.0	29.0
	D_I4	1.008	39.2	30.0
Group II	D_II1	1.013	32.0	24.6
	D_II2	1.009	39.1	29.8
	D_II3	1.009	11.0	8.4
	D_II4	1.008	38.0	29.0
Group III	D_III1	1.003	undeterminate	underteminate
	D_III2	1.007	39.2	30.0
	D_III3	1.003	36	27.4
	D_III4	1.006	39.2	30.0

In agreement with the Griffith criterion,[12] the crack initiation in the Brazilian test for rock and concrete has to be located in the centre of the disk to guarantee the validity of the test. In most of the tests performed in the present research work, the high-speed camera has recorded a sudden appearance of a crack in the centre of the disk, as shown in **Figure 7a** for disk DI_2. However, when the crack is detected it is difficult to ensure that it started in the center. It can be confirmed that the crack starts in the central zone, but not the exact point where it occurs. On the other hand, it was observed that in the disk DII_3, the failure occurs at the edge of the contact arc, as seen in **Figure 7b**. According to **Table 3**, the contact angle for the disk D_II3 is approximately eight degrees. As this contact is smaller than 20º, the failure initiation in the centre of the disk is not guaranteed.[4,6–8,57] Therefore, it is important to pay special attention to the initial contact arc between the disk and the jaws before starting the test. However, in four of the disks a premature failure was detected in the contact zone (**Figure 7c**), even if the final contact angle is greater than 20º.

Moreover, disk D_I1 presents a coexistence of the central crack and cracks on the edges (**Figure 7d**). However, the temporal analysis of the images recorded by the high-speed camera, indicate that the central crack appears before the ones in the contact zone. It has also been observed that the central crack tends to propagate towards the crackled edge, as was observed from previous research studies.[6,8,58]

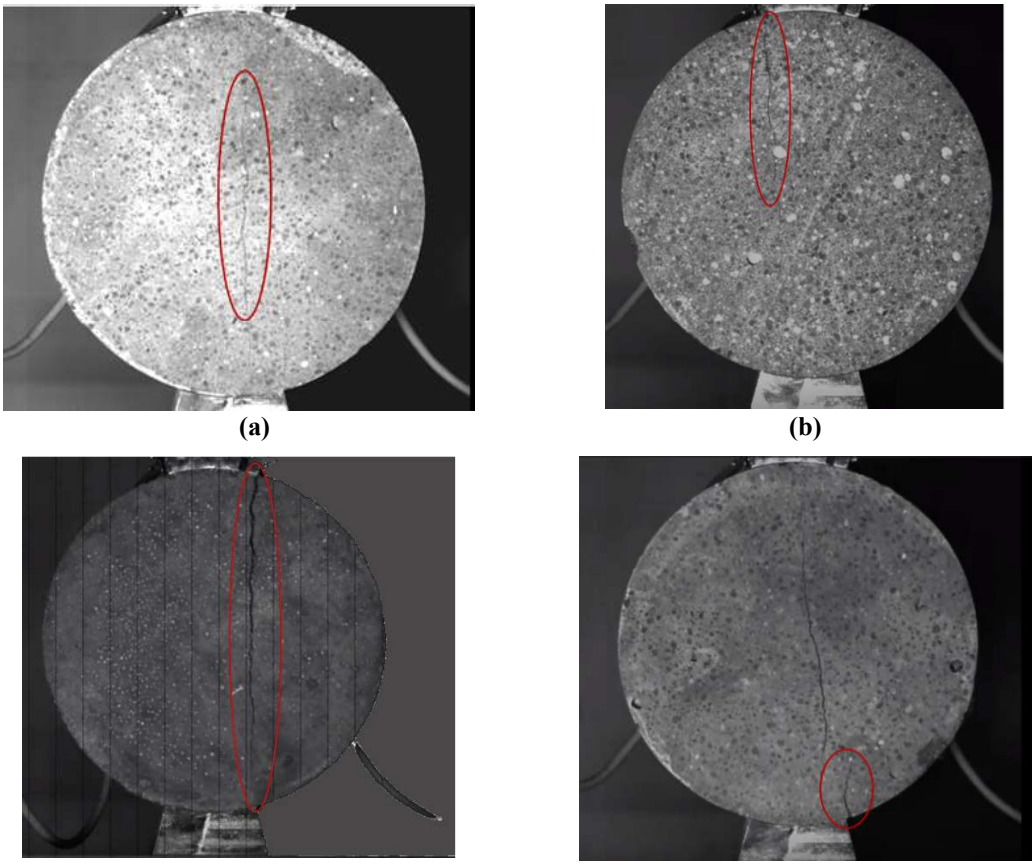

(a) **(b)** **(c)** **(d)**

Figure 7 Different failure mode of concrete Brazilian disk sample tested with loading arc of 30º

According to Komurlu et al.[14] the Brazilian test should be stopped when the first crack has been detected, because the value of the load can change between the crack initiation and the final failure of the disk and therefore, the calculus of the tensile strength with the final load would be incorrect.

During this research work, it has been observed that just when the crack appears, there is usually a fluctuation in the force value registered by the testing machine (**Figure 8a1)**, although this is not always the case (**Figure 8a2** and **8a3)**. It has been seen that in five of the samples, it was not possible to detect the load failure of the disk from the force recorded. **Figure 8a** and **8b** show the records of force from the testing machine and the strain of one of the gauges near the contact, respectively for the time of the disk failure.

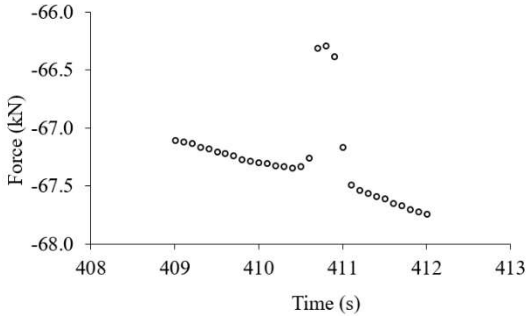

(a1) D_I1

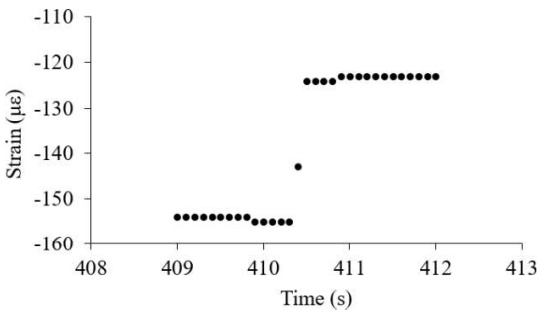

(b1) D_I1

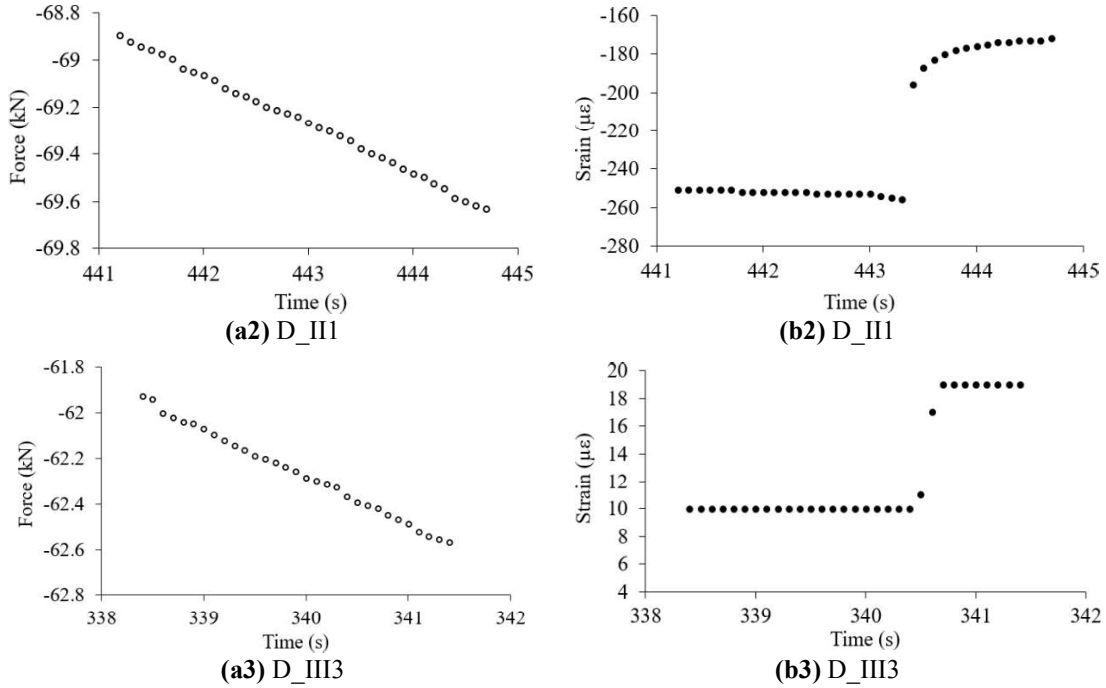

(a2) D_II1 **(b2)** D_II1

(a3) D_III3 **(b3)** D_III3

Figure 8 a Time-dependent force records and **b** strain values experienced by the most deformed gauge at the time of disk failure for the samples D_I1, D_II1 and D_III3.

It has been observed that the strain gauge bonded to the upper loading arc subjected to greater deformations tend to change its value abruptly just when the crack appears (**Figure 8b**). This behavior is systematic since initially, the strains are stable and then they increase or decrease quickly just when the crack appears in the disk. This behavior was also noted by Aliabadian et al.[20] The authors used three strain gauges in different points of the loading diameter of a sandstone Brazilian disk. They observed an abrupt change in the strain measured by the gauges just at the time of disk failure. In the actual research work, instead of instrumenting the disk, the loading arc has been instrumented; therefore, the strain gages can be used many times. **Table 4** shows the magnitudes of the compressive load at the time of disk failure, obtained both with the testing machine and the strain gauges measurements.

Table 4. Failure load detected by the testing machine and by the strain gages measurement

Group number	Disk number	Failure load (kN)	
		Testing machine	Strain gauges
Group I	D_I1	-69.75	-69.75
	D_I2	-73.18	-73.18
	D_I3	-67.34	-67.34
	D_I4	-72.78	-72.78
Group II	D_II1	No detected	-69.32
	D_II2	No detected	-46.62
	D_II3	-48.12	-48.12
	D_II4	No detected	-67.96
Group III	D_III1	-120.00 (Not detected)	-86.60
	D_III2	-68.58	-68.46
	D_III3	No detected	-62.39
	D_III4	-58.371	-58.37

As it can be seen from the results of **Table 4**, only for group I, all the compressive forces corresponding to the crack initiation could be determined with the force-time records of the testing machine. However, thanks to the high sensitivity of the strain gauges, the load corresponding with the crack initiation could be

determined for all the cases. If we compare both force results in the disks of group I, it can be concluded that the instrumentation of the loading arcs with strain gauges can be a low-cost, effective and reliable method to detect the crack initiation load. It has been also possible to verify that the load corresponding to the first crack detected is different from the final failure load of the disk. This coincides with the observations of Komurlu et al.[14] and Rodriguez at al.[42] It should also be noted that in several research papers using the DIC technique,[20,59,60] the maximum registered load is related to the maximum deformation. Therefore, it is very important to determine the crack initiation load, something that, as we have seen, is not always detected by the testing machine.

From the experimental results shown in **Table 4**, it can be deduced that there is a relationship between the dispersion of the crack initiation force values and the sand concentration of the sample. All the samples belonging to group I have failed in the center of the disk, this is why the crack initiation load values are analogous with both methods. However, for group II (sand concentration 20% greater than group I), it can be seen that there is a higher dispersion of results. In the samples D_II1 and D_II4 a central crack was observed, it is for that reason that the values of the failure load are similar. Therefore, these values correspond with the failure strength of the disk since they fulfill the Griffith criterion.[12] On the other hand, in samples D_II2 and D_II3, the crack initiation was located near to one of the contact edges and after was propagated to the center. Therefore, the values of these loads cannot be used to calculate the indirect tensile strength, because they don´t fulfill the failure criterion.

For the third disks group, two of them presented a central crack (D_III2 and D_III3) while for disk D_III4 a premature failure near the contact edge was observed. Special attention must be paid to disk D_III1, since a large difference can be observed between the failure load detected by the testing machine and the one measured with the strain gauges (See **Table 4**). During the test of this specimen, there was no initial crack, nevertheless, an unusual behavior was observed. When the compressive force was greater than 83 kN, the strain in the gauges began to decrease as if the applied load had decreased. It was then decided to continue with the test until the detection of cracks. However, at 120kN, there was a catastrophic failure of the disk that could not be detected with the high-speed camera. **Figure 9** shows the failure of the disk D_III1.

(a) **(b)**

Figure 9 Failed disk sample D_III1

The behavior of the disk D_III1 is not entirely clear but it could be related to the additional sand content of this group. As the sand content in the mix increases, the disk becomes less rigid. **Table 5** shows the average stiffness values for each of the analyzed concrete groups with their respective standard deviation for a 95% confidence level. As it can be seen, the increase in sand concentration causes a decrease in the stiffness of the Brazilian disk. It is also observed that there is an increase in the dispersion of stiffness values as the sand river content increases in the mix.

Table 5. Final stiffness of the concrete Brazilian disk

Group number	Stiffness (kN/mm)
Group I	145.88 ± 2.06
Group II	133.31 ± 5.16
Group III	123.22 ± 6.05

The decrease of the stiffness could explain that at a certain compression load, the disk presents a higher deformation in the contact zone than in the rest, until the edges of the loading devices penetrate in the disk. This would explain the decrease in the strain gauge measurement during the test of disk D_III1. Therefore, the test for this specimen finishes when the behavior of the gauges begins to be unusual, as they inform us that disk failure has occurred even though it cannot be appreciated externally.

According to the results obtained so far, the sand content of the concrete disk affects to the success of the Brazilian test with loading arcs.

4.2. Verification of the probable contact pressure distribution of the concrete disk

In this research work, it has been observed that the use of this type of compression jaws, does not guarantee that the effective contact angle is equal to the loading arc length, since it seems to depend on the elastic properties of the tested material and on the quality of the initial contact between the disk and the jaw. Once the load of failure has been determined, the next step is to determine the indirect tensile strength of the Brazilian disk. There are different analytical and empirical models that allows to calculate this stress,[6,22] as long as the crack initiation is located in the centre of the disk. These models depend on the final contact angle and the pressure distribution in the contact. Gutiérrez et al.[15] demonstrated through simulations with the finite element method that the load distribution in the contact zone is not uniform, even if the contact angle coincides with the loading arc.

Figure 10 presents the most representative transverse and radial strain measurement at the upper loading arc. Different types of load distributions where found from the strain measurements: asymmetrical parabolic **Figure 10(a1-b1)**, symmetrical parabolic **Figure 10(a2-b2)** and asymmetrical punch **Figure 10(a3-b3)**. It can be deduced that, if ρ is greater than one and the initial load is symmetrically applied the load distribution tends to be parabolic. On the other hand, if the initial load is not well aligned with the vertical radius, then the distribution load will be asymmetrical parabolic or punch.

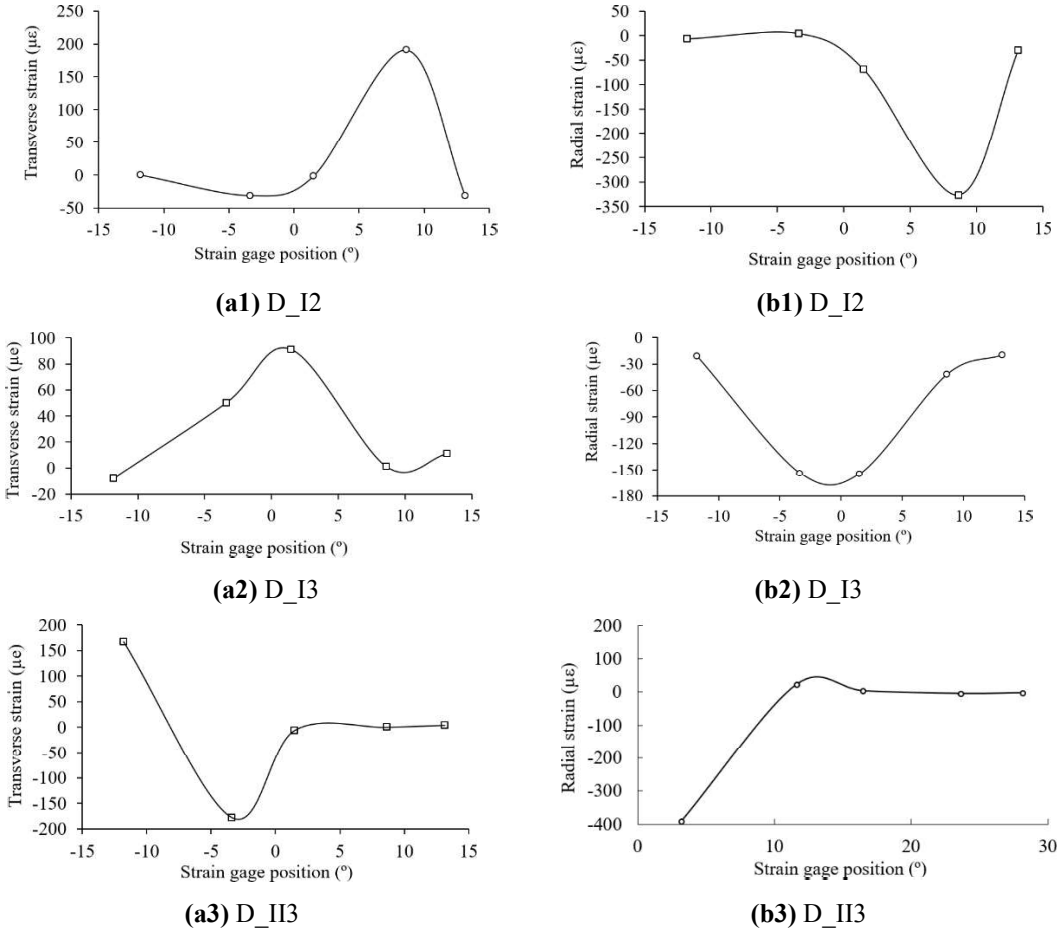

Figure 10 Distribution of: **a** transverse strain and **b** radial strain recorded by the stacked rosette strain gages

Table 6 presents a summary of the results, indicating the radii ratio, the pressure distribution and the initial location of the crack for each tested disk. It can be deduced that, for the group I, the distribution of the contact pressure does not affect to the location of the initial crack. Moreover, for this group, the relative standard deviation of the failure loads shown in **Table 4** is the lowest of the sample (3.88%). However, for groups II and III it can be observed that when the distribution is parabolic the crack occurs in the centre, while a punch distribution increases the premature failure of the disk in the contact edge. It could therefore

be concluded that the success of the concrete tensile test with loading arcs depends on the sand concentration of the mix and on the type of contact distribution pressure.

The results of the strain gauges indicate that the distribution of the load changes with the set-up of the disk in the loading arcs. This set up depends mainly on the surface finish of the parts involved and their geometric tolerances.

Table 6. Effective contact angle calculated from the measurement of the length of the contact arc

Group number	Disk number	ρ (mm/mm)	Possible pressure distribution	Initial crack location
Group I	D_I1	1.007	**Asimetric punch distribution**	Center
	D_I2	1.006	Asimetric parabolic distribution	Center
	D_I3	1.007	Parabolic distribution	Center
	D_I4	1.008	**Asimetric punch distribution**	Center
Group II	D_II1	1.013	Asimetric parabolic distribution	Center
	D_II2	1.009	Asimetric parabolic distribution	Center
	D_II3	1.009	**Asimetric punch distribution**	Edge contact
	D_II4	1.008	**Asimetric punch distribution**	Edge contact and center
Group III	D_III1	1.003	**Asimetric punch distribution**	Edge contact
	D_III2	1.007	**Asimetric punch distribution**	Center
	D_III3	1.003	Asimetric parabolic distribution	Center
	D_III4	1.006	**Asimetric punch distribution**	Edge contact

4.3. Verification of the possible contact pressure distribution with the steel disk

Figure 11 shows the distributions of the transverse and radial strains measurement made by the strain gauges of the upper loading arc. It can be seen that, although there is a complete contact between the loading arcs and the disk (**Figure 4b**), the distribution of the strains are not symmetrical and they increase at the contact edges. The strains shown suggests that when the test boundary conditions are close to the ideal ones, the pressure distribution in the contact is not uniform, as observed in a previous research.[15]

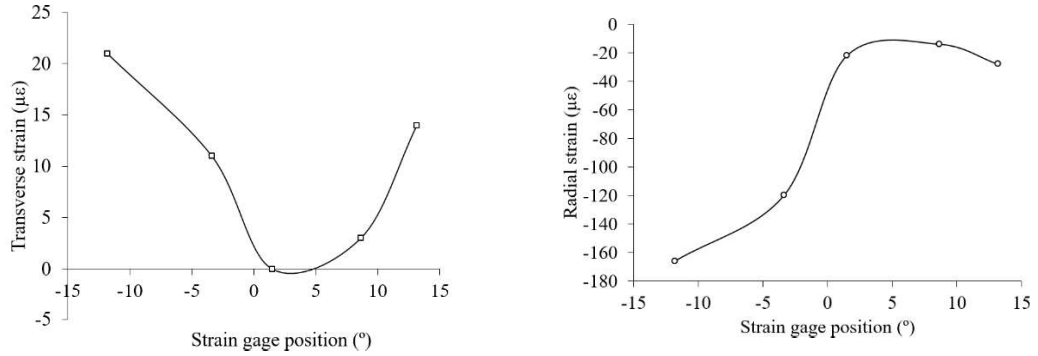

(a) **(b)**

Figure 11 Distribution of: **a** transverse strain and **b** radial strain recorded by the stacked rosette strain gages

The distributions obtained in the concrete and steel disks, indicate that it is complicated to reproduce experimentally the ideal application of the force that is, perfectly centred and vertical. However, according to the results obtained so far in this research work, it can be deduced there can be two types of contact pressure distributions generating the crack in the centre of the disk. The punch distribution is more probable when there is a complete contact from the beginning of the test, whereas the parabolic distribution occurs when the radius of the disk is smaller than the loading arcs and the edges are not initially in contact with the disk. These two distributions can only happen if the load is symmetrically applied. If not, the final pressure distribution will be punch asymmetrical or parabolic asymmetrical.

5. Numerical results

5.1. Verification of the numerical model

In all the simulations results, it was confirmed that the predominant failure condition is $3\sigma_\theta + \sigma_r < 0$, which is in agreement with several research works,[11,15,22]. Therefore, the tensile strength can be given by the equivalent Griffith's stress:[12]

$$\sigma_G = -\frac{(\sigma_\theta - \sigma_r)^2}{8(\sigma_\theta + \sigma_r)} \quad (1)$$

where, σ_θ and σ_r are the transverse and radial stresses respectively.

To confirm that the developed finite element models are well defined, it is necessary to compare the computational results with experimental ones. Therefore, the computational results of the model have been compared with the experimental results obtained by Jin et al.[58] in Brazilian tests with loading arc of 20º. The authors studied the influence of the specimen size on the tensile strength for concrete and mortar disks. The elastic modulus of the concrete and mortar calculated by the authors were 30.32 GPa and 27.45 GPa, respectively. The Poisson ratio for both materials disk was 0.18.

Table 7 shows the experimental tensile strength range obtained by Jin et al.[58] for a confidence level of 95% and the numerical simulations results from our finite element model.

Table 7. Comparative analysis of the numerical simulations with the experimental results of Jin et al.[58]

Diameter (mm)	Thickness (mm)	Failure load (kN)		Tensile strength at the centre of the disk (MPa) [58]		Tensile stress from our simulations (MPa)	
		Concrete	Mortar	Concrete	Mortar	Concrete	Mortar
70	30	8.71	11.44	[2.5 □ 2.8]	[3.5 – 3.7]	2.5	3.4
	55	15.71	20.26	[2.5 □ 2.7]	[3.2 - 3.5]	2.4	3.2

In **Table 7** it can be seen that the results of the finite element model developed in the actual research work, are within the range of the experimental tensile strengths for both material disks tested by these authors.

The simulations results also has been compared with those obtained by Erarslan et al.[6] for different contact angles. The simulations results of Erarslan et al. include the heterogeneity of the mechanical properties of the rock in the numerical model. The authors proved that the simulation results correctly characterize the real fracture behaviour of the tested rock. The sample used by these authors was a Brisbane tuff Brazilian disk with a diameter of 52 mm and a thickness of 26 mm. The loads used were 14.81 kN, 19.20 kN and 22.30 kN for loading arc of 15º, 20º and 30º, respectively. The comparative analysis is shown in **Table 8.**

Table 8. Comparison analysis of indirect tensile strength between the Erarslan et al.[6] results and the simulations of this research work

Loading arc angle (º)	Indirect tensile strength (MPa)[6]	Indirect tensile strength from our simulations (MPa)	Absolute relative difference between both solutions
15	8.04	8.20	2.0%
20	8.29	8.45	1.9%
30	8.70	8.64	0.7%

According to the results of Table 8, it can be concluded that the heterogeneity of the material disk does not significantly affect the final value of the indirect tensile strength.

Erarslan et al.[6] also obtained the experimental indirect tensile strength of Brisbane tuff. To do so, the authors use the empirical expression (2) between the mode I fracture toughness K_{IC} and the tensile strength of rock σ_t for the loading arc configuration that guarantees the central crack of the disk (20º and 30º)

$$K_{IC} = 0.27 + 0.107\sigma_t \quad (2)$$

The experimental indirect tensile strength obtained by the authors was 8.55 MPa for a fracture toughness of this type of rock of K_{IC} = 0.18 MPa·m$^{1/2}$. According to Table 8 it can be verified that this experimental value is in agreement with the results of our simulations.

Therefore, it is verified that the computational model developed in this research work is suitable for the analysis and the calculus of the indirect tensile stress in the Brazilian disk with loading arcs.

5.2. Verification of the effective contact angle from the simulations results

The numerical simulations allow to verify the influence of the elastic, mechanical and geometrical properties of the disk in the effective contact angle. **Table 9** shows the results of the computational design. Of the 26 simulations carried out, only 10 of them present an effective contact angle almost equal to the loading arcs. This is in agreement with the experimental results of the concrete disk and confirm that this alternative method does not guarantee that the effective contact angle will be equal to the loading arc. The final angles from the simulations coincide in most cases with the angles measured on the disks tested. For instance, for the greatest value of radii ratio (ρ =1.013) of the concrete disks, the effective contact angle calculated was 24.6º (**Table 3**). At the same time, in the simulated Brazilian disks for a similar ratio (ρ= 1.014), the final contact angle was 23.3º ± 0.1º for seven of the runs, except for run number 23 (with the lowest Young´s modulus).

Table 9. Results of the Central Composite Design for the verification of the effective contact angle

Run number	E (GPa)	ν ($\mu\varepsilon/\mu\varepsilon$)	σ_t (MPa)	ρ (mm/mm)	2α (°)
1	50	0.25	6	1.002	30
2	30	0.2	4	1.008	30
3	70	0.2	8	1.008	30
4	30	0.3	8	1.008	30
5	70	0.2	4	1.008	22.10
6	70	0.3	8	1.008	28.42
7	70	0.3	4	1.008	22.10
8	30	0.3	4	1.008	30
9	30	0.2	8	1.008	30
10	50	0.15	6	1.014	22.10
11	50	0.25	2	1.014	13.42
12	50	0.25	6	1.014	22.10
13	50	0.35	6	1.014	22.10
14	50	0.25	6	1.014	23.23
15	90	0.25	6	1.014	18.95
16	50	0.25	10	1.014	28.42
17	10	0.25	6	1.014	30
18	70	0.3	4	1.02	13.42
19	70	0.3	8	1.02	18.95
20	30	0.3	8	1.02	26.84
21	70	0.2	8	1.02	18.95
22	30	0.3	4	1.02	18.95
23	70	0.2	4	1.02	13.42
24	30	0.2	8	1.02	26.84
25	30	0.2	4	1.02	18.95
26	50	0.25	6	1.026	17.37

An ANOVA analysis with the statistical Statgraphic Centurion software has been performed to study the variability of the effective contact angle. The statistical parameters resulting from the analysis of the variance of the results of **Table 9** indicate that the Young's modulus of the disk, the maximum tensile strength and the radii ratio ρ are significant for a 95% confidence level, i.e. they have an influence in the magnitude of the final contact angle. However, there is no influence of the Poisson´s ratio, at least for the ranges considered.

Of the influencing factors, the radii ratio is the only factor that we can control since it depends on the machining of the disks. For this reason, we have analyzed the influence of the Young's Modulus together with the maximum tensile strength on the three radii ratios 1.008, 1.014 and 1.02 indicated in **Table 9.**

Figure 12 shows the response surface of the effective contact angle for these radii ratios considering the joint interaction of the Young's modulus and maximum tensile strength from the computational design.

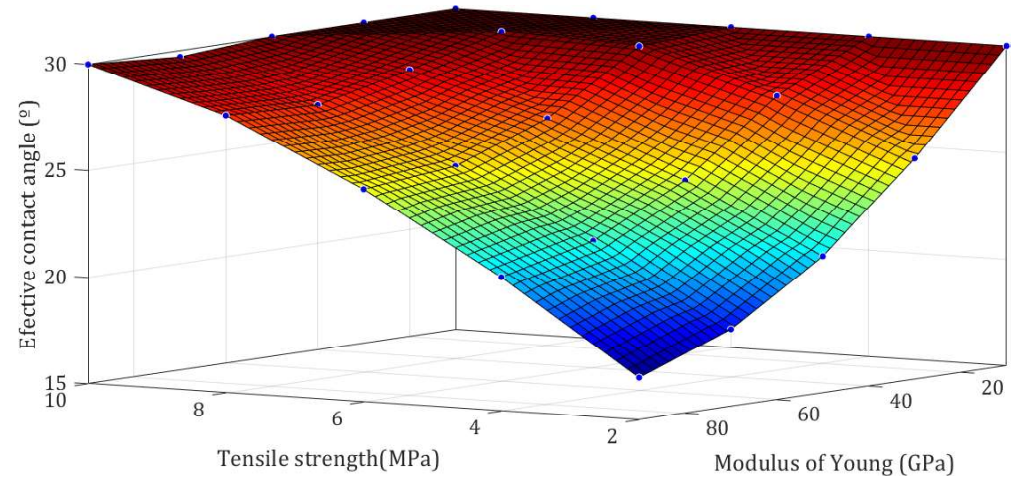

(a)

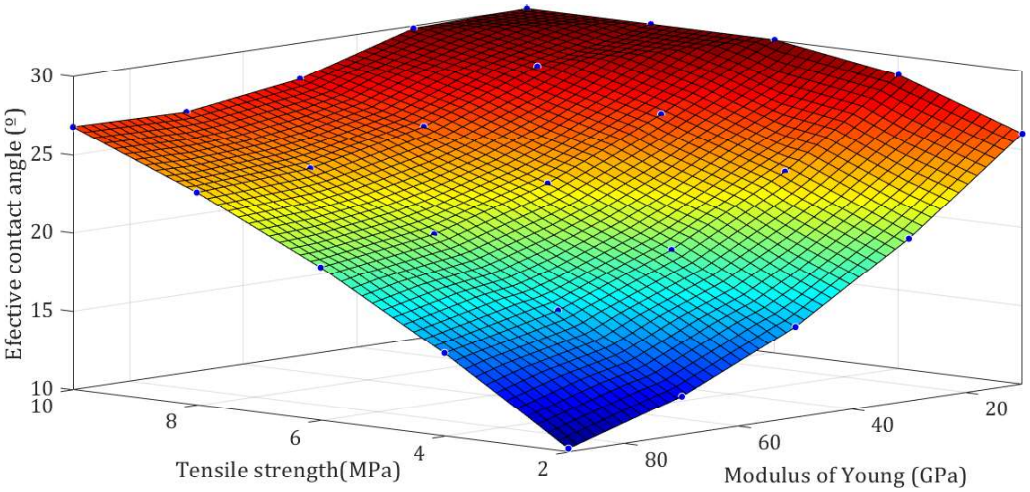

(b)

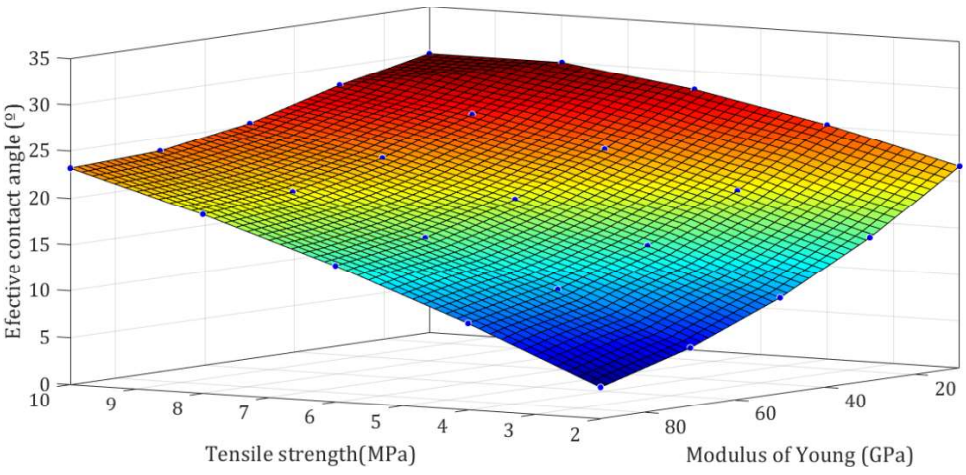

(c)

Figure 12 Variability of the effective contact angle for the radii ratio of: **a** 1.008, **b** 1.014 and **c** 1.02

In **Figure 12,** it can be seen that the variability of the effective contact angle depends on the mechanical and elastic properties of the disk tested. This variability is small in materials with low Young's modulus (less than 20 GPa), that is for rocks like soft and medium sandstone, coal and shale.[61]

On the other hand, when the Brazilian test with loading arc is performed on materials with a higher Young's modulus ($E \geq 60$ GPa) as hard sandstone, marble and limestone,[61,62] a better control in disk preparation is necessary. It is only for $\rho = 1.008$ and tensile strengths greater or equal to 8 MPa (**Figure 12**

a) that the contact angle correspond to the loading device (30º) at the moment of the central failure of the disk.

The results of the computational study carried out in this research work show a quite complex scenario to analytically determine the value of the effective contact angle. As was mentioned before, in a real Brazilian test with loading arcs it is possible to know the effective contact angle if the test is stopped just when the first crack appears. The experimental results show that this is possible if the upper loading arc is instrumented with strain gauges, since the abrupt change in the behavior of these gauges just before the failure of the disk has been found to be systematic. Furthermore, the marks caused by the pressure exerted by the loading arcs in the contact area of the disk allow to measure the arc length, and thus, the effective contact angle.

5.3. Computational verification of the possible failure mode of concrete Brazilian disk ~~sample~~ tested with loading arc of 30º

According to several research works, ,[11,15,22] when the tensile strength is given by the equivalent Griffith's stress (1) the probability of premature failure increases as the contact angle decreases. In order to guarantee that the maximum equivalent stress is located in the center of the disk, it is recommended that $2\alpha \geq 20º$. However, in the mentioned research works it is assumed that the load distribution is symmetrical with the vertical diameter of the disk.

Recreating the failure modes observed experimentally in the different concrete disks shown in **Figure 7** by analytical methods is quite complicated. However, it is possible to check how the possible boundary conditions affect to the stress distribution using the finite element model. **Figure 13** shows the numerical simulations of the possible failure modes in term of Griffith stress distribution (1) of the concrete Brazilian disk tested with loading arc of 30º. In all the cases reproduced, the contact condition was imposed at the beginning of the simulation.

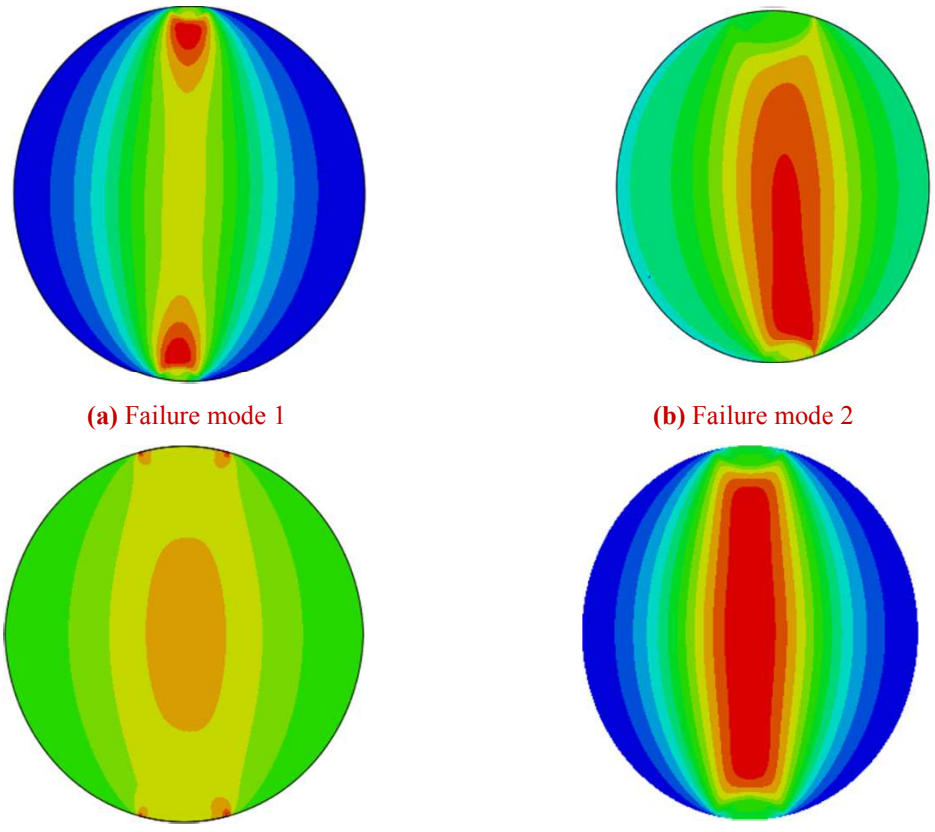

(a) Failure mode 1 **(b)** Failure mode 2

(c) Failure mode 3 **(d)** Failure mode 4

Figure 13 Possible failure mode of the concrete Brazilian disk sample tested with loading arc of 30º

Figure 13a shows the distribution of the equivalent tensile stress for a disk with a diameter tolerance similar to DII_3. In this numerical model, the initial contact was on one of the edges of the loading device. According to the stress distribution shown, the maximum stresses are present in the contact area, which causes the premature failure of the disk in this zone as it was observed in the real concrete disks tested DI_2 and DII_3 (**Figure 7b** and **Figure 7c**, respectively). On the other hand, if the initial contact is only half the

arc length of the loading arc, because a misalignment of the load has been generated, the maximum equivalent stresses occur between the contact zone and the center of the disk (**Figure 13b**). Therefore, there is a high probability that the failure mode resembles that of disk D_I1 (**Figure 7d),** which presents a central crack and also cracks on the contact edge. The final contact angle, according to the simulation, is the same that the loading devices but the contact pressure distribution is not symmetrical. This result demonstrates the importance of setting up self-aligned loading devices as the misalignment of the arcs can produce this type of failure mode in a higher or lower degree.

Another possible failure mode is shown in **Figure 13c**, where cracks may occur in the contact edges together with a central crack. This failure could be present when the loading arcs penetrate the disk because the radius of the disk is slightly larger (0.1 mm) than the loading arcs. We believe that in this case, small cracks could appear at the contact edges as well as a central crack as was observed on the disk DII_3 (**Figure 7c**). Moreover, it is possible that in a real test two cracks appears along the entire disk between the upper and lower contact edges as the disk D_III1 (**Figure 9a**).

Figure 13d show the numerical tensile stress distribution for the disk DI_3. According to the stress distribution from the simulation result, in a real test it is probable to observe a sudden appearance of a crack in almost the entire vertical diameter of the disk, as shown in **Figure 7a**, because the stresses in this zone are similar.

6. Uncertainty point of view of the crack initiation

According to the results seen so far and the observations of other research works,[6,7,14] it seems very difficult to observe experimentally the exact location of the crack initiation point in the Brazilian disk. It is assumed that when a central crack is visualized, the failure criterion required in this type of test is met. Moreover, the probabilistic engineering field has demonstrated that everything around us has a stochastic nature.[63,64] That is why this section quantifies the uncertainty of the stress along the loading diameter of the Brazilian disk in order to explain why it is complicated to verify experimentally the crack initiation point.

For this purpose, the uncertainties of the input variables of the analytical Brazilian stress models are quantified. The latest will consider the punch and parabolic contact pressure distributions deduced from the experiments.

6.1. Theoretical models

Considering that the contact between the loading arcs and the disk shown in **Figure 14** is small ($a \ll R$),the state of the stress at any arbitrary point M inside the Brazilian disk can be expressed as the superposition of:[65]

- The stress due to the contact pressure distribution between the top and the bottom loading devices and the disk.
- A distributed uniform tensile stress applied on the boundary of the disk (3):

$$\sigma_u = \frac{P}{\pi R t} \tag{3}$$

where P is the applied load, α is the semi-loading angle, R is the radius of the flattened disk and t is the thickness of the disk.

In the actual study, the contact surfaces are supposed to be shear traction free. The stresses inside the disk can be obtained by the superposition of two concentrated forces $p(s)$ acting normal to the surfaces on an infinitesimal area of length ds. Therefore, the equivalent stress components for an arbitrary point M can be calculated by solving the following integrals:[65]

$$\sigma_{xr} = -\frac{2y_1}{\pi}\int_{-b}^{a}\frac{p(s)(x-s)^2}{\left[(x-s)^2+y_1^2\right]^2}ds - \frac{2y_2}{\pi}\int_{-b}^{a}\frac{p(s)(x-s)^2}{\left[(x-s)^2+y_2^2\right]^2}ds \tag{4}$$

$$\sigma_{yr} = -\frac{2y_1^3}{\pi}\int_{-b}^{a}\frac{p(s)}{\left[(x-s)^2+y_1^2\right]^2}ds - \frac{2y_2^3}{\pi}\int_{-b}^{a}\frac{p(s)}{\left[(x-s)^2+y_2^2\right]^2}ds \tag{5}$$

$$\tau_{xyr} = -\frac{2y_1^2}{\pi}\int_{-b}^{a}\frac{p(s)(x-s)}{\left[(x-s)^2+y_1^2\right]^2}ds - \frac{2y_2^2}{\pi}\int_{-b}^{a}\frac{p(s)(x-s)}{\left[(x-s)^2+y_2^2\right]^2}ds \tag{6}$$

where r_1 and r_2 are the distances between the upper and lower infinitesimal lengths *ds* and point *M*, *s* is the horizontal distance from the vertical axis to *ds,* and y_1 and y_2 are the vertical distances between the upper and lower contact surfaces and point *M,* respectively.

Once the distribution *p(s)* is known, then the final state of the stresses inside the Brazilian disk can be calculated via the integration of expressions (4), (5) and (6) along the loaded zone and superimposing the uniform tensile stress on the boundary of the disk (3).

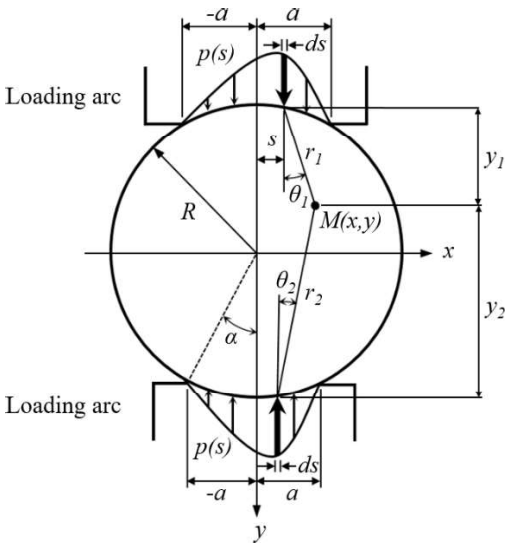

Figure 14 Theoretical contact of the Brazilian disk with loading arcs

If the pressure in the contact is described by a rigid punch distribution, then *p(s)* is defined as follows:[65]

$$p_{ch}(s) = \frac{P}{\pi t\left(a^2 - s^2\right)^{1/2}} \tag{7}$$

On the other hand, if the pressure in the contact is described by a parabolic distribution then *p(s)* is:[65]

$$p_p(s) = \frac{2P}{\pi a^2 t}\left(a^2 - s^2\right)^{1/2} \tag{8}$$

where *P* is the applied load, *t* is the disk thickness, and *a* and *s* are the edge and an arbitrary point position, respectively.

Considering the pressure distribution (7) into equations (4), (5) and (6) and superposing the uniform tensile stress (3), the expressions for the calculus of the stress field for the loading diameter of the Brazilian disk for the punch distribution are:

$$\sigma_{\theta ch} = \frac{P}{\pi Rt}\left\{1 - R\left[\frac{a^2}{\left(a^2 + y_1^{\,2}\right)^{3/2}} + \frac{a^2}{\left(a^2 + y_2^{\,2}\right)^{3/2}}\right]\right\} \tag{9}$$

$$\sigma_{rch} = \frac{P}{\pi Rt}\left\{1 - R\left[\frac{a^2 + 2y_1^{\,2}}{\left(a^2 + y_1^{\,2}\right)^{3/2}} + \frac{a^2 + 2y_2^{\,2}}{\left(a^2 + y_2^{\,2}\right)^{3/2}}\right]\right\} \tag{10}$$

$$\tau_{\theta rch} = 0 \tag{11}$$

where, from **Figure 14** we have:

$$\begin{aligned} a &= R\alpha \\ y_1 &= R - r \\ y_2 &= R + r \end{aligned} \tag{12}$$

Being *r* any arbitrary point of the vertical radius

Repeating the previous procedure, but this time for the parabolic pressure distribution (8), the expressions for the calculus of the stress field in the loading diameter of the disk will be:

$$\sigma_{\theta p} = \frac{P}{\pi R t}\left\{1 - \frac{2R}{a^2}\left[\frac{a^2 + 2y_1^{\,2}}{\left(a^2 + y_1^{\,2}\right)^{1/2}} + \frac{a^2 + 2y_2^{\,2}}{\left(a^2 + y_2^{\,2}\right)^{1/2}} - 2\left(y_1 + y_2\right)\right]\right\} \tag{13}$$

$$\sigma_{rp} = \frac{P}{\pi R t}\left\{1 - \frac{2R}{a^2}\left[\frac{a^2}{\left(a^2 + y_1^{\,2}\right)^{1/2}} + \frac{a^2}{\left(a^2 + y_2^{\,2}\right)^{1/2}}\right]\right\} \tag{14}$$

$$\tau_{\theta p} = 0 \tag{15}$$

Once the transverse σ_θ and radial σ_r stresses for the two pressures distribution considered have been calculated, the tensile strength will be given by the equivalent Griffith's stress (1).

6.2. Statistic comparison tool

The uncertainty quantification of the theoretical models was developed using the Monte Carlo methods following the procedure recommended by the Guide for the expression of the uncertainty in measurement (GUM).[66] **Table 10** shows the values of the uncertainties of the measurement tools used with their respective probability density function. For the radius and the thickness, their final uncertainty is a combined uncertainty that considers the value of **Table 10** and standard deviation of the measurements.

Table 10 Uncertainties of the theoretical variables

Variable	Units	Uncertainty u	Probability density function
P	N	$8.75\times10^{-3}P$	Normal
R	mm	5.78×10^{-2}	Normal
t	mm	2.89×10^{-2}	Normal
2α	Radians	1.00×10^{-3}	Rectangular

The normalized error[67] has been calculated to identify the points of the vertical radius with stresses equivalent to the maximum tensile strength, considering a confidence level of 95%. The reference value will be the maximum tensile stress calculated in the vertical radius of the disk and this will be compared with the stresses in different points of the radius.

The normalized error is a statistical tool that allows to compare two results when the uncertainty of both is taken into account.[68] Thus, it can be said that the two results represent the same phenomena or measurand if the normalized error score is less than one. The normalized error for the case study was defined as:

$$E_N = \frac{\left|\sigma_{G\_\max} - \sigma_{G\_r}\right|}{\sqrt{U^2\left(\sigma_{G\_\max}\right) - U^2\left(\sigma_{G\_r}\right)}} = \frac{\left|\sigma_{G\_\max} - \sigma_{G\_r}\right|}{\sqrt{\left(\frac{\sigma_{G\_\max h} - \sigma_{G\_\max l}}{2}\right)^2 - \left(\frac{\sigma_{G\_rh} - \sigma_{G\_rl}}{2}\right)^2}} \tag{16}$$

where:

- σ_{G_max} is the maximum equivalent Griffith's stress.
- σ_{G_maxh} and σ_{G_maxl} are respectively the lower and upper limits of the probable values of the maximum equivalent Griffith's stress for a coverage level of 95%.
- σ_{G_r} = is the equivalent Griffith's stress for any arbitrary point of the vertical radius.
- σ_{G_rh} and σ_{G_rl} are the lower and upper limits of σ_{G_r} for a coverage level of 95%.

6.3. Results of the statistical comparison

Figure 15a1 and **Figure 15b1** show the statistical comparison analysis developed with the two analytical models (section 6.1), considering the punch distribution and parabolic distribution on the pressure contact respectively. The input data of the models correspond the disks D_I3 and D_III3. The points in red color in the vertical diameter are those complying with $E_N < 1$, and therefore represent the same measurand, that is, the same equivalent stress. Moreover, **Figure 15a2** and **Figure 15b2** show the crack location in disks D_I3 and D_III3, in which the punch and parabolic pressure distributions are better exemplified. As it can be seen, the theoretical representations are in agreement with the experimental ones.

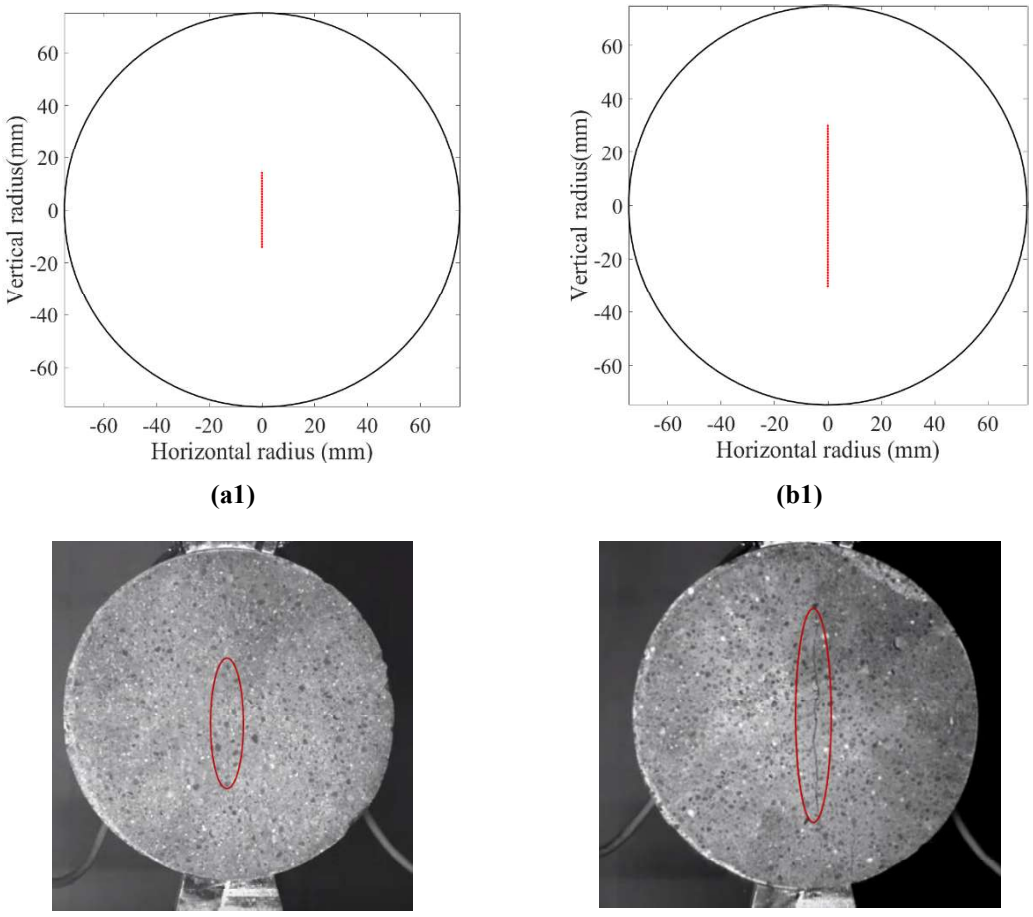

Figure 15 Crack location in the vertical diameter of the disk for the contact pressure distributions: **a** punch and **b** parabolic, for a contact angle of 30º

In **Figure 15** it can be seen that when the uncertainties of the input data considered in theoretical solution are taken into account, it is possible to understand why it is complicated to experimentally verify the failure initiation point in the disk. **Figure 15a1** and **Figure 15b1**, confirm with a confidence of level of 95% that the points of the disks indicated in red are submitted to the same maximum stress. Therefore, there is a probability of 95% that the crack will appear suddenly in this segment of the diameter as it can be seen in the tested specimens of **Figure 15a2** and **Figure 15b2**.

The fact that the crack initiation point cannot be observed even with a high-speed camera does not mean that the test is not valid; on the contrary, it justifies that the failure criterion is fulfilled because a central crack is detected. According to the results of **Figure 15**, the type of contact pressure distribution seems to have an influence in the initial length of the crack. In the theoretical solution with the punch distribution, the crack is smaller than the one obtained with the parabolic distribution (**Figure 15a1** and **Figure 15b1,** respectively).

Figure 16 shows the points of the vertical diameter for different contact angles that present an E_n number (16) less than one, and therefore, have equivalent tensile stress magnitude. It can be appreciated that the model based on parabolic distribution (**Figure 16b**) is more sensitive to the variation of the contact angle than the punch distribution (**Figure 16a**). Within the range of angles studied, the latest fulfils the Griffith´s criterion. On the other hand, it has been observed that for the parabolic distribution and a contact angle of 20º (**Figure 16b2**), there is a 95% probability of observing two additional cracks together with the central crack. If the angle is less than 20º (**Figure 16b3**), the parabolic distribution does not comply any longer with the failure criterion.

The results shown in **Figure 16** coincide with the conclusions of Aliabadian et al.[21] They observed with Digital Image Correlation techniques that a first crack line might initiate in the disk centre or somewhere between the contact zone and the centre. Moreover, Fourmeau et al.[36] observed also a first central crack line using a high speed camera and DIC analysis technique in the study of granite rock disks, demonstrated by the uncertainty analysis carried out in the actual research work.

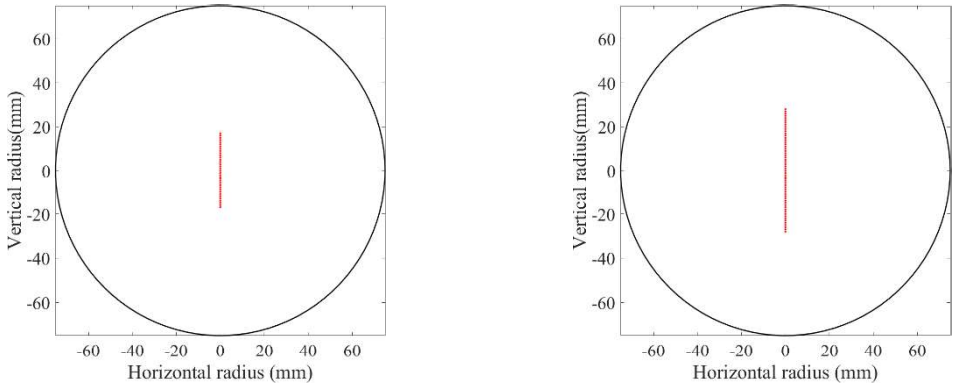

(a1) 25º **(b1)** 25º

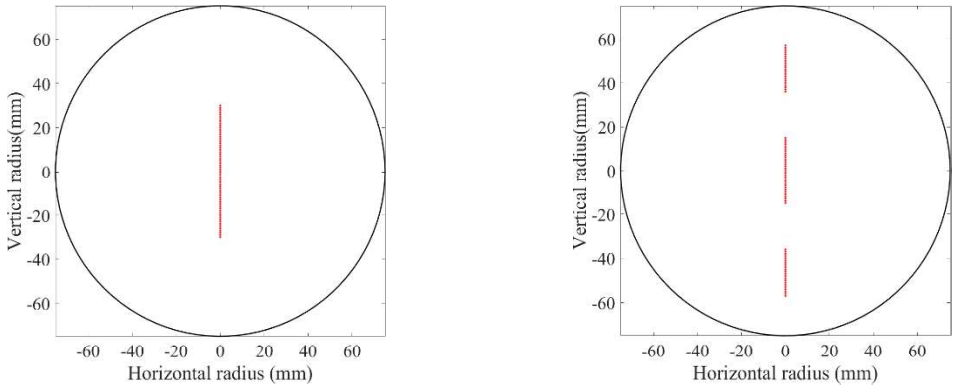

(a2) 20º **(b2)** 20º

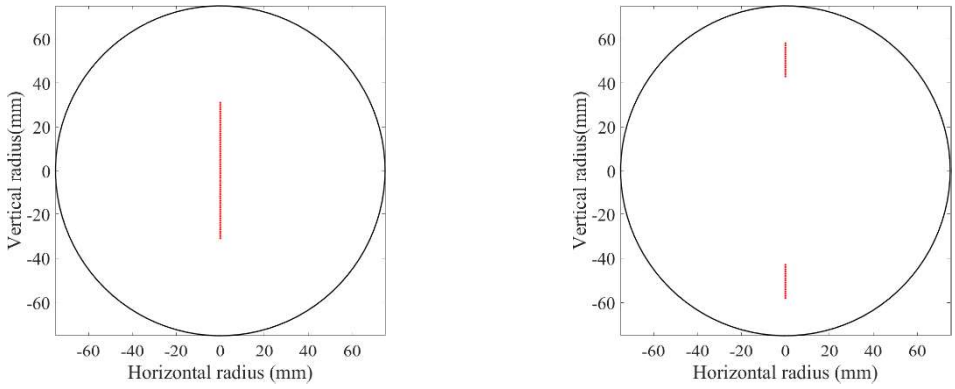

(a3) 19º **(b3)** 19º

Figure 16 Possible **c**rack location in the vertical diameter of the disk for the contact pressure distributions: **a** punch and **b** parabolic, in function of the contact angle value.

7. Determination of the indirect tensile strength

The distribution of the pressures in the contact zone measured by the strain gauges for the 12 concrete disks do not meet completely the conditions described in the models of section 6.1. However, according to the Saint-Venant principle[69] the influence of the loading distribution tends to dissipate as the distance from the loading area increases. This principle is demonstrated in **Figure 17** as it shows the evolution of the transverse and radial stresses in the vertical radius of the steel disk for a compression load of 40 kN. The stresses have been calculated after the strains measured with the gauges bonded on the steel disk (**Figure 4a**). It can be observed that between the position 0 mm/mm and 0.5 mm/mm (centre and middle point of the radius) both stresses tend to stabilize.

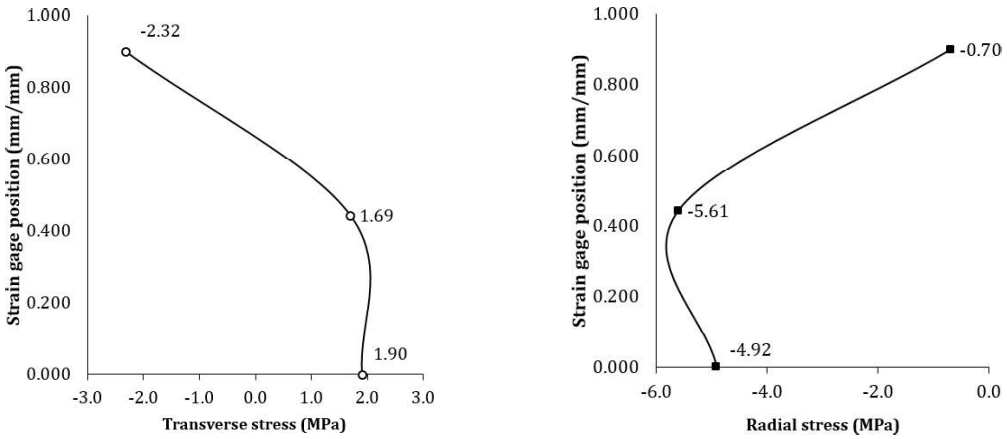

Figure 17 Evolution of the transverse **a** and radial stresses **b** calculated from the strain measured in the Brazilian steel disk

Considering that, the properties of the material disk do not significantly affect the results of the splitting tensile strength for the same load magnitude,[70] **Table 11** shows the results of the tensile stress calculated from the strain gauges measurements, together with the results of the simulations and the analytical solutions considered, for a confidence level of 95 %. The uncertainty of the experimental stress was calculated following the recommendation given by GUM.[48] This combined uncertainty considers both the experimental standard deviation of the five repetitions of the Brazilian test and the uncertainty of the material properties. The uncertainty contribution of the strain gage measurements was not quantified, as it was previously verified in a recent research that it could be neglected.[70] The numerical solution have been considered as deterministic.

Table 11 Comparison of the experimental tensile stress in the centre of the steel disk with the theoretical and numerical solutions for a confidence level of 95%

Experimental tensile stress (MPa)	Numerical tensile stress (MPa)	Theoretical solutions	
		Punch distribution	Parabolic distribution
1.90 ± 0.2	1.91	1.92 ± 0.06	2.06 ± 0.06

The results shown in **Table 11** indicate that both the numerical solution and the analytical solution correspond to the experimental tensile stress in the centre of the steel disk. The analytical solution with the punch distribution is the one closer to furthest from the experimental result, because the pressure distribution determined with the strain gauges (**Figure 11**) is more similar to a punch type than to a parabolic one.

Before calculating the indirect tensile strength on the disks tested, additional non-destructive test was made with an extra concrete disk M80, in order to compare its result with the available theoretical solution. The selected disk is the one that had the best dimensional characteristic of all the manufactured disks. The disk has a diameter of 150.09 mm and a thickness of 75.1 mm, with a standard deviation of the geometrical magnitudes inferior to 0.15%. It was verified that the specimen fitted the loading device correctly, to increase the probability of having a symmetrical contact pressure distribution.

For the comparative analysis, the load applied was 29.9 kN ± 0.55 kN in order to avoid the failure of the specimen. A stacked rectangular rosette of 6 mm-grid length has been bonded in the disk centre aligned with the transverse and radial direction (**Figure 18**). Five repetition of the indirect test were carried out to calculate an equivalent tensile stress (1) in the centre of the disk to check the repeatability.

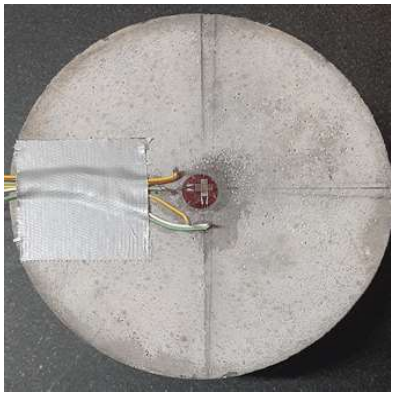

Figure 18 Instrumented concrete disk

The Young's modulus has been calculated from the value of the compressive strength f_c with the following equation:[71,72]

$$E = 4.73\sqrt{f_c} \tag{17}$$

The compressive strength of disk was 82 MPa and its modulus of elasticity calculated with equation (17) was 45.3 GPa ± 5%. The Poisson coefficient used was 0.15 with a variability of ±0.05 according to the state of the art.[71,73]

Table 12 presents the comparative analysis between the tensile stress measured in the centre of the concrete disk and the numerical and theoretical results for a confidence level of 95%.

Table 12 Comparison of the experimental tensile stress in the centre of the concrete disk M80 with the numerical and theoretical solutions for a confidence level of 95%

Experimental tensile stress (MPa)	Numerical tensile stress (MPa)	Theoretical solutions	
		Punch distribution	Parabolic distribution
1.50 ± 0.11	1.55	1.43 ± 0.08	1.52 ± 0.08

In **Table 12**, it can be seen that the numerical and analytical results have both values in common with the experimental tensile stress when the uncertainties of the magnitudes are taken into account. The best prediction corresponds to the analytical expression with the parabolic distribution, as the strains registered by the instrumented loading arc indicate a parabolic pressure distribution.

After the comparative analysis carried out on the steel disk and the concrete disk, it can be concluded that the theoretical models and the finite elements solution represents the experimental tensile stress in the disk centre for a confidence level of 95%.

Table 13 shows the results of the indirect tensile strength with their respective combined uncertainty for the concrete disks presenting a central crack. The stresses have been calculated for the two principal contact pressure distributions observed during the test. The magnitude of the contact angle chosen for each disk corresponds to the values showed in **Table 3**. Additionally, the results of the finite element simulation for each disk have been included. For the calculus of the finite element solution, it was supposed that the Young's modulus of the concrete disk of group II and group III change according to the stiffness (**Table 5**). Therefore, the modulus of elasticity for these concrete disk groups are 41.38 GPa and 38.24 GPa, respectively.

Table 13. Final indirect tensile strength of the Brazilian concrete disk that comply with the failure criterion

Group number	**Disk number**	**Indirect tensile strength (MPa)**		
		Finite element solution	**Punch distribution**	**Parabolic distribution**
Group I	D_I1	3.65	3.48 ± 0.08	3.66 ± 0.08
	D_I2	3.81	3.68 ± 0.14	3.89 ± 0.14
	D_I3	3.53	3.29 ± 0.08	**3.54 ± 0.08**
	D_I4	3.83	3.74 ± 0.12	3.82 ± 0.12

Group II	D_II1	3.68	3.47 ± 0.10	3.73 ± 0.10
	D_II2	2.45	2.32 ± 0.06	2.46 ± 0.06
Group III	D_III2	3.56	3.15 ± 0.05	3.28 ± 0.05
	D_III3	3.10	3.12 ± 0.08	3.32 ± 0.09

In **Table 13** it can be observed that all the samples of group I present analogous indirect tensile strengths. The reference tensile strength corresponds to disk D_I3, since it is the one that is closer to the ideal conditions in terms of symmetric contact pressure distribution (**Figure 10(a2-b2)**). The mean indirect tensile strength of group I is 3.73 MPa with an expanded uncertainty of 0.19 MPa (95% of confidence level). The uncertainty is calculated considering the uncertainty of each stress value shown in **Table 13** and the experimental standard deviation of the mean, according to GUM,[48] The results of this group have shown acceptable repeatability.

For the result of the rest of the groups, the sample size of the valid Brazilian concrete disk tested is insufficient for statistical inference. In both groups, the effectiveness of the test technique used is 50%, therefore it is necessary to increase the sample size in order to characterize the mechanical strength of the concrete disks for the group II and III. In this case, it can be said that the contact pressure distribution together with the river sand concentration affects to the validity of this alternative indirect test.

8. Solutions to minimize the negative effect of boundary conditions

According to the state of the art,[6,17,19] the Brazilian test with loading arcs allows to know and control the contact angle from the beginning of the test. However, the results found indicate that as the final set up depends mainly on the surface finish of the parts and their geometric tolerances, it is not always possible to ensure a complete contact angle. If these boundary conditions are met, then it is expected to have a punch type contact pressure distribution.

Unfortunately, it is not always easy the recreate experimentally this ideal condition. First, because even if the contact angle is correct, it is difficult to guarantee a symmetrical distribution of the applied load. This can reduce the success of the test, as it was observed that an asymmetric punch distribution increases the possibility of premature disk failure in the contact edge with higher load applied.

For instance, seven of the twelve tests carried out presented an asymmetric punch distribution but only three of them had a central crack. These results are in agreement with the advice given by Mellor and Hawkes [18] who criticized this loading configuration, claiming that the arc ends could penetrate the disk.

A possible solution to minimise the premature failure would be to use self-centring loading jaws with rounded edges. However, the difficulty of generating a perfect surface finish in the contact zone will always have a negative influence in the contact angle and symmetry of the load.

On the other hand, the five tests with parabolic distribution fulfil the failure criterion. Thus, another possible solution when using this jaw configuration is that the radius of the disk has to be smaller than the loading arcs ($\rho>1$). Moreover, the jaws could incorporate a self-centring device and the set-up must be carefully carried out to ensure that the initial contact zone is not in the edges. This would generate a parabolic type distribution in the contact, preventing a premature disk failure in the edges. In this case, the contact edges apply less pressure in the disk and therefore do not penetrate the sample as the punch distribution does. According to the simulation results, the radii ratio ρ together with the Young modulus and the material strength affect to the final contact angle. To guarantee a centre crack location in the Brazilian disk, the contact angle must be at least 20º. In order to fulfil with this failure criterion, the geometric tolerance has to be more restrictive for material disk with high Young modulus than for material with low Young modulus.

The problem of this configuration is that the magnitude of the final contact is not completely controlled. However, if an angle in the range of 20-30º can be ensured, the variation of the final indirect tensile strength is not so significant compared to the importance of guarantying a central crack. **Table 14** shows the tensile strength values calculated with the two theoretical models from section 6.1 for the contact angles of 20º and 30º. It can be observed that the differences between the resulting stresses for the contact angle range considered are less than 6 %.

Table 14. Comparison of the influence of the contact angle and loading pressure distribution in the calculus of the indirect tensile strength for a confidence level of 95 %

Applied load P (kN)	Contact angle (º)	Diameter (mm)	Thickness (mm)	Final indirect tensile strength (MPa)	
				Punch distribution	Parabolic distribution
80 kN	20 ± 0.17	151.14 ± 0.12	75.30 ± 0.03	4.20 [4.12, 4.36]	4.46 [4.34, 4.58]

	30 ± 0.17			3.97 [3.85, 4.09]	4.22 [4.09, 4.34]

Another possible improvement of this indirect test could be to use loading arc with a smaller angle than 30º. According to the results of the computational models from **Table 9** if instead of using the 30º configuration, a 20º loading arc was chosen, in can be expected that in the majority of the disk tested the final contact angle would correspond to the length of the loading arc. In this configuration, the variability of the contact angle could be reduced by more than a half with respect to the 30º loading arc, meeting at the same time, the requirement to guarantee the central failure of the disk.

For an indirect tensile test with loading arcs, it would be enough to locate three strain gauges on the loading device in order to detect the moment of failure and thus the load and the possible contact pressure distribution.

9. Conclusions

The results found in the experimental test carried out with 12 concrete disks and the numerical simulations has allowed to answer some unsolved questions related to the Brazilian test by means of the following conclusions:

- The instrumentation of the loading arc with strain gauges presented in this research work embodies a new methodology that allows to determine with a high precision the final failure load. This methodology allows to detect the disk failure even when the damage cannot be observed externally.
- The determination of this failure load is not always possible with the universal testing machine so this new testing set-up provides a great advantage with respect to the existing one.
- The increase of the sand concentration in the concrete samples has a negative effect on the quality of the test results, as it increases both the dispersion of the failure load and the stiffness of the disk.
- Relevant aspects of the experimental set-up like the asymmetry of the load, the surface finish and the roundness of the disk are critical to guaranty the success of the test.
- The strain gauge measurements reveal two possible tendencies in the contact load distribution, parabolic and punch type.
- A contact in the edges of the loading arc, since the beginning of the test, increases the premature failure of the disk when it is combined with an asymmetrical load. This is because it tends to concentrate the pressure near these edges.
- This indirect test does not guarantee that the final contact angle will be equal the one of loading arcs.
- The results of the computational study carried out evidence a quite complex scenario to analytically determine the value of the effective contact angle. The variability of the contact angle depends of the mechanical and elastic properties of the material tested.
- The instrumentation used allows to stop the test when the failure load is detected. Therefore, the length of the contact arc can be measured with the marks left by the jaws on the disk surface and the final contact angle can be calculated.
- The uncertainty quantification of the tensile stress for the points of the vertical diameter of the disk demonstrates why a sudden central crack line is observed experimentally instead of a point initiation.
- The type of contact pressure distribution has an influence in the initial length of the crack, but it doesn´t significantly affect to the results of the tensile stress in the centre of the disk, since both solutions are in agreement with the experimental results.
- In order to improve the success of the test it is recommended to use self-centring loading arc of 20º and disks with a radius smaller than the loading arcs ($\rho>1$). Moreover, the set-up must be carefully carried out to ensure that the initial contact zone is not limited to the edges of the loading arcs.

Declaration of interest

The authors declare that they have no conflict of interest.

Acknowledgements

The authors of this paper acknowledge to the company Tubyder S. L. for having supplied the concrete disks that have been tested.

Bibliography

1. Claesson J, Bohloli B. Brazilian test: Stress field and tensile strength of anisotropic rocks using an analytical solution. *Int J Rock Mech Min Sci*. 2002;39(8):991-1004. doi:10.1016/S1365-1609(02)00099-0
2. Mier JGM Van, Vliet MRA Van. Uniaxial tension test for the determination of fracture parameters of concrete : state of the art. *Eng Fract Mech*. 2002;69:235-247.

3. Berenbaum R, Brodie I. Measurement of the tensile strength of brittle materials. *Br J Appl Phys*. 1959;10(6):281-287. doi:10.1088/0508-3443/10/6/307
4. Fairhurst C. On the validity of the "Brazilian" test for brittle materials. *Int J Rock Mech Min Sci*. 1964;1(4):535-546. doi:10.1016/0148-9062(64)90060-9
5. Markides CF, Pazis DN, Kourkoulis SK. Closed full-field solutions for stresses and displacements in the Brazilian disk under distributed radial load. *Int J Rock Mech Min Sci*. 2010;47(2):227-237. doi:10.1016/j.ijrmms.2009.11.006
6. Erarslan N, Liang ZZ, Williams DJ. Experimental and numerical studies on determination of indirect tensile strength of rocks. *Rock Mech Rock Eng*. 2012;45(5):739-751. doi:10.1007/s00603-011-0205-y
7. Li D, Wong LNY. The brazilian disc test for rock mechanics applications: Review and new insights. *Rock Mech Rock Eng*. 2013;46(2):269-287. doi:10.1007/s00603-012-0257-7
8. Komurlu E, Kesimal A. Evaluation of Indirect Tensile Strength of Rocks Using Different Types of Jaws. *Rock Mech Rock Eng*. 2015:1723-1730. doi:10.1007/s00603-014-0644-3
9. Carneiro FLLB. A new method for determining the tension stress in the concrete. Proceedings of 5th Meet of Association Brazilian for Standardization. In: Proceedings of 5th Meet of Association Brazilian for Standardization - ABNT, 3th Section; 1943:126-129. https://scholar.google.com/scholar_lookup?title=+Résistance+à+la+traction+des+bétons+-+Une+nouvelle+méthode+pour+La+détermination+de+La+résistance+à+la+traction+des+bétons&author=Carneiro+F.L.L.B.&publication_year=1. Accessed March 22, 2017.
10. Hondros G. The evaluation of Poisson's ratio and modulus of materials of a low tensile resistance by the Brazilian (indirect tensile) test with particular reference to concrete. *J AppL Sci*. 1959;10:243-268.
11. García VJ, Márquez CO, Zúñiga-Suárez AR, Zuñiga-Torres BC, Villalta-Granda LJ. Brazilian Test of Concrete Specimens Subjected to Different Loading Geometries: Review and New Insights. *Int J Concr Struct Mater*. 2017;11(2):343-363. doi:10.1007/s40069-017-0194-7
12. Griffith AA. The Phenomena of Rupture and Flow in Solids. *Philos Trans R Soc A Math Phys Eng Sci*. 1921;221(582-593):582-593. doi:10.1098/rsta.1921.0006
13. Liu C. Elastic Constants Determination and Deformation Observation Using Brazilian Disk Geometry. *Exp Mech*. 2010;50(7):1025-1039. doi:10.1007/s11340-009-9281-2
14. Komurlu E., Kesimal A., Demir S. Experimental and numerical study on determination of indirect (splitting) tensile strength of rocks under various load apparatus. *Can Geotech J*. 2016;53(2):360-372. doi:10.1139/cgj-2014-0356
15. Gutiérrez-Moizant R, Ramírez-Berasategui M, Santos-Cuadros S, García-Fernández C. Computational Verification of the Optimum Boundary Condition of the Brazilian Tensile Test. *Rock Mech Rock Eng*. 2018;0(0):0. doi:10.1007/s00603-018-1553-7
16. Hudson JA, Brown ET, Rummel F. The controlled failure of rock discs and rings loaded in diametral compression. *Int J Rock Mech Min Sci*. 1972;9(2):241-248. doi:10.1016/0148-9062(72)90025-3
17. Jaeger JC, Hoskins ER. Rock failure under the confined Brazilian test. *J Geophys Res*. 1966;71(10):2651-2659. doi:10.1029/JZ071i010p02651
18. Mellor M, Hawkes I. Measurement of tensile strength by diametral compression of discs and annuli. *Eng Geol*. 1971;5(3):173-225. doi:10.1016/0013-7952(71)90001-9
19. Yu Y, Zhang J, Zhang J. A modified Brazilian disk tension test. *Int J Rock Mech Min Sci*. 2009;46(2):421-425. doi:10.1016/j.ijrmms.2008.04.008
20. Aliabadian Z, Zhao GF, Russell AR. Crack development in transversely isotropic sandstone discs subjected to Brazilian tests observed using digital image correlation. *Int J Rock Mech Min Sci*. 2019;119(November 2018):211-221. doi:10.1016/j.ijrmms.2019.04.004
21. Aliabadian Z, Zhao GF, Russell AR. Failure, crack initiation and the tensile strength of transversely isotropic rock using the Brazilian test. *Int J Rock Mech Min Sci*. 2019;122(July):104073. doi:10.1016/j.ijrmms.2019.104073
22. Satoh Y. Position and Load of Failure in Brazilian Test ; A Numerical Analysis by Griffith Criterion. *J Mater Sci Japan*. 1986;140(36):1219-1224. doi:10.2472/jsms.36.1219
23. Lavrov A, Vervoort A. Theoretical treatment of tangential loading effects on the Brazilian test stress distribution. *Int J Rock Mech Min Sci*. 2002;39(2):275-283. doi:10.1016/S1365-1609(02)00010-2
24. Markides CF, Pazis DN, Kourkoulis SK. Influence of friction on the stress field of the brazilian tensile test. *Rock Mech Rock Eng*. 2011;44(1):113-119. doi:10.1007/s00603-010-0115-4
25. van de Steen B, Vervoort A, Napier JAL. Observed and simulated fracture pattern in diametrically loaded discs of rock material. *Int J Fract*. 2005;131(1):35-52. doi:10.1007/s10704-004-3177-z

26. Cai M, Kaiser PK. Numerical simulation of the Brazilian test and the tensile strength of anisotropic rocks and rocks with pre-existing cracks. *Int J Rock Mech Min Sci*. 2004;41(SUPPL. 1):1-6. doi:10.1016/j.ijrmms.2004.03.086
27. Lanaro F, Sato T, Stephansson O. Microcrack modelling of Brazilian tensile tests with the boundary element method. *Int J Rock Mech Min Sci*. 2009;46(3):450-461. doi:10.1016/j.ijrmms.2008.11.007
28. Olesen JF, Østergaard L, Stang H. Nonlinear fracture mechanics and plasticity of the split cylinder test. *Mater Struct*. 2007;39(4):421-432. doi:10.1617/s11527-005-9018-3
29. Malárics V, Müller HS. Evaluation of the splitting tension test for concrete from a fracture mechanical point of view the. *Proc Fract Mech Concr Concr Struct - Assessment, Durability, Monit Retrofit Concr Struct*. 2010:709-716.
30. Wang SY, Sloan SW, Tang CA. Three-Dimensional Numerical Investigations of the Failure Mechanism of a Rock Disc with a Central or Eccentric Hole. *Rock Mech Rock Eng*. 2013;47(6):2117-2137. doi:10.1007/s00603-013-0512-6
31. Lin H, Xiong W, Zhong W, Xia C. Location of the Crack Initiation Points in the Brazilian Disc Test. *Geotech Geol Eng*. 2014;32(5):1339-1345. doi:10.1007/s10706-014-9800-5
32. Riera JD, Miguel LFF, Iturrioz I. Assessment of Brazilian tensile test by means of the truss-like Discrete Element Method (DEM) with imperfect mesh. *Eng Struct*. 2014;81:10-21. doi:10.1016/j.engstruct.2014.09.036
33. Zhu JB, Liao ZY, Tang CA. Numerical SHPB Tests of Rocks Under Combined Static and Dynamic Loading Conditions with Application to Dynamic Behavior of Rocks Under In Situ Stresses. *Rock Mech Rock Eng*. 2016;49(10):3935-3946. doi:10.1007/s00603-016-0993-1
34. Mahabadi OK, Cottrell BE, Grasselli G. An example of realistic modelling of rock dynamics problems: FEM/DEM simulation of dynamic brazilian test on Barre Granite. *Rock Mech Rock Eng*. 2010;43(6):707-716. doi:10.1007/s00603-010-0092-7
35. Zhang QB, Zhao J. A review of dynamic experimental techniques and mechanical behaviour of rock materials. *Rock Mech Rock Eng*. 2014;47(4):1411-1478. doi:10.1007/s00603-013-0463-y
36. Fourmeau M, Gomon D, Vacher R, Hokka M, Kane A, Kuokkala V-T. Application of DIC Technique for Studies of Kuru Granite Rock under Static and Dynamic Loading. *Procedia Mater Sci*. 2014;3(2211):691-697. doi:10.1016/j.mspro.2014.06.114
37. Zhang QB, Zhao J. Determination of mechanical properties and full-field strain measurements of rock material under dynamic loads. *Int J Rock Mech Min Sci*. 2013;60:423-439. doi:10.1016/j.ijrmms.2013.01.005
38. Zhou Z, Li X, Zou Y, Jiang Y, Li G. Dynamic brazilian tests of granite under coupled static and dynamic loads. *Rock Mech Rock Eng*. 2014;47(2):495-505. doi:10.1007/s00603-013-0441-4
39. Malyszko L, Bilko P, Kowalska E. Determination of Elastic Constants in Brazilian Tests Using Digital Image Correlation. *Proc - 2017 Balt Geod Congr (Geomatics), BGC Geomatics 2017*. 2017:153-157. doi:10.1109/BGC.Geomatics.2017.73
40. He W, Chen K, Zhang B, Dong K. Improving measurement accuracy of Brazilian tensile strength of rock by digital image correlation. *Rev Sci Instrum*. 2018;89(11). doi:10.1063/1.5065541
41. Ai D, Zhao Y, Xie B, Li C. Experimental Study of Fracture Characterizations of Rocks under Dynamic Tension Test with Image Processing. *Shock Vib*. 2019;2019:1-14. doi:10.1155/2019/6352609
42. Rodríguez P, Arab PB, Celestino TB. Characterization of rock cracking patterns in diametral compression tests by acoustic emission and petrographic analysis. *Int J Rock Mech Min Sci*. 2016;83(December 2017):73-85. doi:10.1016/j.ijrmms.2015.12.017
43. Zhang SW, Shou KJ, Xian XF, Zhou JP, Liu GJ. Fractal characteristics and acoustic emission of anisotropic shale in Brazilian tests. *Tunn Undergr Sp Technol*. 2018;71:298-308. doi:10.1016/j.tust.2017.08.031
44. Wang J, Xie L, Xie H, et al. Effect of layer orientation on acoustic emission characteristics of anisotropic shale in Brazilian tests. *J Nat Gas Sci Eng*. 2016;36:1120-1129. doi:10.1016/j.jngse.2016.03.046
45. European Committee for Standardization. EN 197-1:2011 Cement Part 1: Composition, Specifications and Conformity Criteria for Common Cements. *Eur Stand*. 2011:50. doi:doi:10.3403/30205527U
46. Mibei G. Presented at Short Course IX on Exploration for Geothermal Resources, INTRODUCTION TO TYPES AND CLASSIFICATION OF ROCKS. 2014:1-12.
47. Mubiayi MP. Characterisation of sandstones: Mineralogy and physical properties. *Lect Notes Eng Comput Sci*. 2013;3 LNECS(July):2171-2176.
48. Joint Committee for Guides in Metrology (JCGM). Evaluation of measurement data: Guide to the expression of uncertainty in measurement. 2008;(September):120.

doi:10.1373/clinchem.2003.030528
49. Gabauer W. The Determination of Uncertainties in Tensile Testing. *Man Codes Pract Determ Uncertainies Mech tests Met Mater*. 2000;(1):35. http://www.npl.co.uk/upload/pdf/cop07.pdf. Accessed July 16, 2018.
50. Micro-Measurements V. *Strain Gage Rosettes: Selection, Application and Data Reduction*. Vol 11065.; 2008.
51. ASTM International. ASTM E111-04 Standard Test Method for Young's Modulus, Tangent Modulus, and Chord Modulus. 2004. doi:10.1520/E0111-04
52. ASTM International. ASTM E132-04 Standard Test Method for Poisson's Ratio at Room Temperature. 2010. doi:10.1520/E0132-04R10
53. Indriyantho BR, Nuroji. Finite element modeling of concrete fracture in tension with the Brazilian splitting test on the case of plane-stress and plane-strain. *Procedia Eng*. 2014;95(Scescm):252-259. doi:10.1016/j.proeng.2014.12.185
54. Burak E, Ahmet T. Determination of Frictional Behaviour Between Concrete and Steel Tube Interaction. 2014;(September).
55. Simulia DS. *Abaqus Documentation*.; 2016. http://abaqus-users.1086179.n5.nabble.com/ABAQUS-REFERENCE-td18129.html. Accessed March 23, 2017.
56. Khuri AI, Mukhopadhyay S. Response surface methodology. *Wiley Interdiscip Rev Comput Stat*. 2010;2(2):128-149. doi:10.1002/wics.73
57. Wang QZ, Jia XM, Kou SQ, Zhang ZX, Lindqvist PA. The flattened Brazilian disc specimen used for testing elastic modulus, tensile strength and fracture toughness of brittle rocks: Analytical and numerical results. *Int J Rock Mech Min Sci*. 2004;41(2):245-253. doi:10.1016/S1365-1609(03)00093-5
58. Jin X, Hou C, Fan X, et al. Quasi-static and dynamic experimental studies on the tensile strength and failure pattern of concrete and mortar discs. *Sci Rep*. 2017;7(1):1-15. doi:10.1038/s41598-017-15700-2
59. Stirling RA, Simpson DJ, Davie CT. The application of digital image correlation to Brazilian testing of sandstone. *Int J Rock Mech Min Sci*. 2013;60:1-11. doi:10.1016/j.ijrmms.2012.12.026
60. Belrhiti Y, Dupre JC, Pop O, et al. Combination of Brazilian test and digital image correlation for mechanical characterization of refractory materials. *J Eur Ceram Soc*. 2017;37(5):2285-2293. doi:10.1016/j.jeurceramsoc.2016.12.032
61. Molina O, Vilarrasa V, Zeidouni M. Geologic Carbon Storage for Shale Gas Recovery. *Energy Procedia*. 2017;114(September):5748-5760. doi:10.1016/j.egypro.2017.03.1713
62. Jianhong Y, Wu FQ, Sun JZ. Estimation of the tensile elastic modulus using Brazilian disc by applying diametrically opposed concentrated loads. *Int J Rock Mech Min Sci*. 2009;46:568-576. doi:10.1016/j.ijrmms.2008.08.004
63. Chen W, Baghdasaryan L, Buranathiti T, Cao J. Model Validation via Uncertainty Propagation and Data Transformations. *AIAA J*. 2004;42(7):1406-1415. doi:10.2514/1.491
64. Hills RG, Leslie IH. Statistical validation of engineering and scientific models: validation experiments to application. *Sandia Tech Rep*. 2003;(SAND2003-0706).
65. Johnson KL. *Contact Mechanics*. Vol 108.; 1985. doi:10.1115/1.3261297
66. Joint Committee for Guides in Metrology. *JCGM 101: Evaluation of Measurement Data — Supplement 1 to the "Guide to the Expression of Uncertainty in Measurement" — Propagation of Distributions Using a Monte Carlo Method*.; 2008.
67. Gutiérrez R, Ramírez M, Olmeda E, Díaz V. Practical Case Application for Stress Model Validation and Enhancement by Means of Metrological Tools. *Strain*. 2015;51(5):379-390. doi:10.1111/str.12149
68. ISO 13528. *Statistical Methods for Use in Proficiency Testing by Interlaboratory Comparison*. Switzerland; 2015.
69. F. LNG. A Treatise on the Mathematical Theory of Elasticity. *Nature*. 1920;105(2643):511-512. doi:10.1038/105511a0
70. Gutiérrez-Moizant R, Ramírez-Berasategui M, Santos-Cuadros S, García-Fernández CC. A Novel Analytical Solution for the Brazilian Test with Loading Arcs. *Math Probl Eng*. 2020;2020(c). doi:10.1155/2020/2935812
71. Toma IO, Covatariu D, Toma AM, Taranu G, Budescu M. Strength and elastic properties of mortars with various percentages of environmentally sustainable mineral binder. *Constr Build Mater*. 2013;43:348-361. doi:10.1016/j.conbuildmat.2013.02.061
72. Jurowski K, Grzeszczyk S. The influence of concrete composition on Young's modulus. *Procedia Eng*. 2015;108:584-591. doi:10.1016/j.proeng.2015.06.181
73. Barbosa CS, Lourenço PB, Hanai JB. On the compressive strength prediction for concrete masonry

prisms. *Mater Struct Constr*. 2010;43(3):331-344. doi:10.1617/s11527-009-9492-0